International Journal of Solids and Structures 171 (2019) 30–46

Contents lists available at ScienceDirect

International Journal of Solids and Structures

journal homepage: www.elsevier.com/locate/ijsolstr

Modeling the axial-torsional response of metallic strands accounting for the deformability of the internal contact surfaces: Derivation of the symmetric stiffness matrix

Francesco Foti*, Luca Martinelli

Politecnico di Milano, Department of Civil and Environmental Engineering, P.zza L. da Vinci 32, Milano 20133, Italy

ARTICLE INFO

Article history:
Received 28 January 2019
Revised 23 April 2019
Available online 8 May 2019

Keywords:
Strands
Axial-torsional loads
Hertzian contact
Curved thin-rod theory

ABSTRACT

A new formulation for the evaluation of the axial-torsional response of single-layer metallic strands is presented. The proposed model fully accounts for the contraction of the helix radius of the external wires due to both the Poisson effect and the local deformation (flattening) of the internal contact surfaces. Closed form equations are found for the coefficients of the cross sectional elastic stiffness matrix of the strand. Differently from other models of the literature that include the effects of the radial contraction of the wire helices, the proposed stiffness matrix is symmetric. The proposed expressions for the terms of the stiffness matrix are remarkably compact and simple, making them an attractive tool for analytical developments and design calculations. Extensive comparisons with experimental, analytical and Finite Element results of the literature show that the proposed expressions are accurate over a wide range of strand constructions and within a loading range sufficiently extended to cover most practical service conditions.

1. Introduction

Metallic strands are lightweight and efficient structural components, widely employed to carry large axial loads in many different civil and mechanical engineering systems, such as suspended bridges, deployable structures, cranes, lifting devices for mining and offshore applications. Strands are made of concentric layers of metallic wires, helically wound around an initially straight central wire (also called the *core wire*). A review of the most common strand typologies can be found in Feyrer (2007). The most simple strand geometry, which is nevertheless often adopted in the applications, employs a single layer of metallic wires with circular cross section. This will be considered in the present work.

The axial-torsional experimental behavior of metallic strands is characterized, for service loads (i.e. up to about 40% of the rated tensile strength), by being substantially linear elastic and by the coupling between the axial and torsional response, due to the helicoidal shape of the wires (see e.g.: Utting and Jones, 1987a; Utting and Jones, 1987b; Cappa, 1988; Kumar and Botsis, 2001; Onur, 2016).

Several mechanical models have been proposed in the literature to describe the axial-torsional behavior of strands, see e.g. the reviews in Cardou and Jolicoeur (1997) and Spak et al. (2013). They can be broadly subdivided, on the base of the mechanical model adopted to describe the wires inside the strand, into: semi-continuous and discrete formulations. The first ones are based on homogenization procedures to replace the layers of wires with an equivalent elastic continuum, such as an orthotropic thin layer in plane stress state (e.g. Raoof and Hobbs, 1988) or a three-dimensional cylinder made of orthotropic material (e.g. Blouin and Cardou, 1989). Discrete models, instead, are based on the individual modeling of each wire of the strand as a curved thin rod.

The accuracy of semi-continuous models improves at the increase of the number of layers and the number of components per layer, hence they can be conveniently applied to describe large diameter strands with many layers of external wires. On the other hand, discrete models have been found to deliver more reliable results for the most common case of strands made of one or few layers of external wires (Raoof and Kraincanic, 1994). Hence a discrete model is better suited to deal with the simple geometry of the single layer strand herein investigated.

A review of the literature related to discrete models reveals that neglecting the changes in the strand internal geometry related to the contraction of the helix radius of the external wires

* Corresponding author.
E-mail addresses: francesco.foti@polimi.it (F. Foti), luca.martinelli@polimi.it (L. Martinelli).

https://doi.org/10.1016/j.ijsolstr.2019.05.008
0020-7683/

(e.g. Machida and Durelli, 1972; Sathikh et al., 1996; Foti and Martinelli, 2016) leads to an overestimation of the elastic stiffness terms. A better estimate under axial-torsional loads is possible if the Poisson effect and the compliance of the internal contact surfaces between the external wires and the core one (also termed *wire flattening*) is fully accounted for. However, inclusion of these aspects can considerably increase the complexity of the mechanical formulation, making numerical solution strategies, such as finite elements (e.g. Jiang et al., 1999; Ghoreishi et al., 2007; Judge et al., 2012; Xiang et al., 2017), an interesting option. Finite Element (FE) formulations, however, while providing an invaluable tool to investigate complex local mechanical phenomena (e.g. wear and fretting fatigue phenomena) cannot be successfully applied to large-scale structural analyses, or iterative design computations, because of their computational costs.

Several attempts have been made in the past to include the contraction of the wire helix radius into analytical formulations. Geometrically non linear models, accounting for the radial contraction induced by Poisson effect, have been proposed by Huang (1978) and Costello and coworkers (summarized in Costello (1990)). This last model has been later linearized by Velinsky et al. (1984) and also by Kumar and Cochran (1987). An early attempt to include both the radial contraction due to the Poisson effect and the wire flattening has been made by Utting and Jones (1987a,b) through an empirical approach that avoided solving the contact problem. A more refined formulation has been proposed by Argatov (2011), considering the contact between all the external wires and the core one through an application of the method of matched asymptotic expansions (Argatov, 2001). More recently, semi-analytical solutions were proposed by Meng et al. (2016) and Chen et al. (2017).

All the previous formulations, which take into account the change in internal geometry, were typically obtained by stating the mechanical problem in a geometrically non linear framework, and subsequently by linearizing it. However, whenever this has been done, a non-symmetric stiffness matrix was obtained, which violates Betti's reciprocal work theorem, that is at the very base of elastic systems. A recent exception is the model of Karathanasopoulos and Kress (2015), who have studied the response of helical rods subjected to axial-torsional loads and an imposed radial contraction, obtaining a symmetric stiffness matrix. However, differently from the previously reviewed works, in their formulation the radial strain is considered as an external loading condition, i.e. it is not induced by the Poisson and flattening effects. This model has then been applied to the study of the effect of thermal loads in stranded conductors by Karathanasopoulos et al. (2016).

A novel approach is proposed in this work to model the axial-torsional response of single layer strands, accounting in an energetically consistent way for the contraction of the helix radius of the external wires due to both the Poisson and flattening effect. The proposed formulation, which leads for the first time within this context (to the authors' knowledge) to a symmetric stiffness matrix, is based on: a) the individual modeling of the wires as linear elastic curved thin rods, b) the modeling of the interaction between the external wires and the core wire as an Hertzian normal contact problem, and c) a comprehensive internal non-linear kinematic model that relates the generalized strains of the wires to the ones of the strand, fully accounting for both the flattening and Poisson effect. This is subsequently linearized to express the strain energy of the strand in closed form, leading to remarkably compact and simple equations for the terms of the elastic stiffness matrix.

The outcomes of the proposed formulation are assessed against available experimental results, well established analytical models and FE models from the literature.

The effects of different modeling approaches for the contact compliance are also systematically investigated in a wide range of strand geometries to assess their impact on the strand response.

2. Geometry of the strand

This paper focuses on metallic strands made of a single layer of wires with circular cross section, helically twisted around a cylindrical core wire. The core of the strand is assumed to be straight in the reference (undeformed) configuration and the number of external wires is denoted as n_w (see Fig. 1(a)). The most common strand construction currently adopted in civil and mechanical engineering applications is the 1/6 one, characterized by six external wires (i.e.: $n_w = 6$) wrapped around a core wire (see Fig. 1(b) and (c)).

2.1. Geometry of the helical wires

The geometry of the wires surrounding the cylindrical core can be conveniently described in a Strand-attached Reference System (SRS). To this aim, a right-handed Cartesian set of axes $\{x_k\}$ with unit vectors $\{\mathbf{e}_k\}$ $(k = 1, 2, 3)$ can be defined, such that the axis x_1 coincides with the strand centerline. Within this framework, the centerline of the external wires is described as a circular helix (of radius R_0 and pitch P_0) by the following position vector:

$$\mathbf{x}_0 = \frac{P_0}{2\pi}\left(\theta - \theta|_{x_1=0}\right)\mathbf{e}_1 + R_0\cos(\theta)\mathbf{e}_2 + R_0\sin(\theta)\mathbf{e}_3 \tag{1}$$

where θ is the *swept angle* of the helix (i.e. the angle defined by the axis x_2 with the projection on the plane $x_1 = 0$ of the vector $\mathbf{x}_0$, as shown in Fig. 1(a)), while the symbol $\theta|_{x_1=0}$ is adopted to denote the value of the swept angle on the plane $x_1 = 0$. Please notice that in Eq. (1) and in the rest of this work the subscript '0' is adopted to identify geometric variables defined in the reference configuration of the problem.

Starting from Eq. (1), the Serret–Frenet unit vectors $\{\mathbf{f}_k(\theta)\}$ $(k = 1, 2, 3)$ of the helix can be easily evaluated (see e.g. Kreyszig, 1991) and adopted to define the orientation of the cross sections of the wires with respect to the SRS. The Serret–Frenet unit vectors can be related to the ones of the SRS by means of a rotation tensor, $\mathbf{\Lambda}_0(\theta)$, such that:

$$\mathbf{f}_k(\theta) = \mathbf{\Lambda}_0(\theta)\mathbf{e}_k, \quad k = 1, 2, 3 \tag{2}$$

By denoting as $\mathbf{f}_1$, $\mathbf{f}_2$ and $\mathbf{f}_3$, respectively: the tangent, normal and binormal unit vector of the wire centerline (see also Fig. 1(b)), the components of the rotation tensor in the SRS can be collected in the matrix $\mathbf{\Lambda}_{0,\mathbf{e}_k}(\theta)$:

$$\mathbf{\Lambda}_{0,\mathbf{e}_k}(\theta) = \begin{pmatrix} \cos(\alpha_0) & 0 & \sin(\alpha_0) \\ -\sin(\alpha_0)\sin(\theta) & -\cos(\theta) & \cos(\alpha_0)\sin(\theta) \\ \sin(\alpha_0)\cos(\theta) & -\sin(\theta) & -\cos(\alpha_0)\cos(\theta) \end{pmatrix} \tag{3}$$

where α_0 is the lay angle of the wire, i.e. the constant angle between the tangent vector $\mathbf{f}_1$ and the centerline of the strand (axis x_1). By considering the development of the wire centerline on a planar surface (i.e. the projection, without stretching or shrinking, of the wire centerline on a plane (see e.g. Lee (1991))), the lay angle α_0 can be easily related to the radius (R_0) and pitch (P_0) through the following trigonometric relation: $\alpha_0 = \arctan\left(\frac{2\pi R_0}{P_0}\right)$. Starting from Eq. (1), then, the normal curvature (κ_0) and torsion (τ_0) of the wire centerline can be evaluated, respectively, as (see e.g. Kreyszig, 1991):

$$\kappa_0 = \frac{\sin^2(\alpha_0)}{R_0} \tag{4}$$

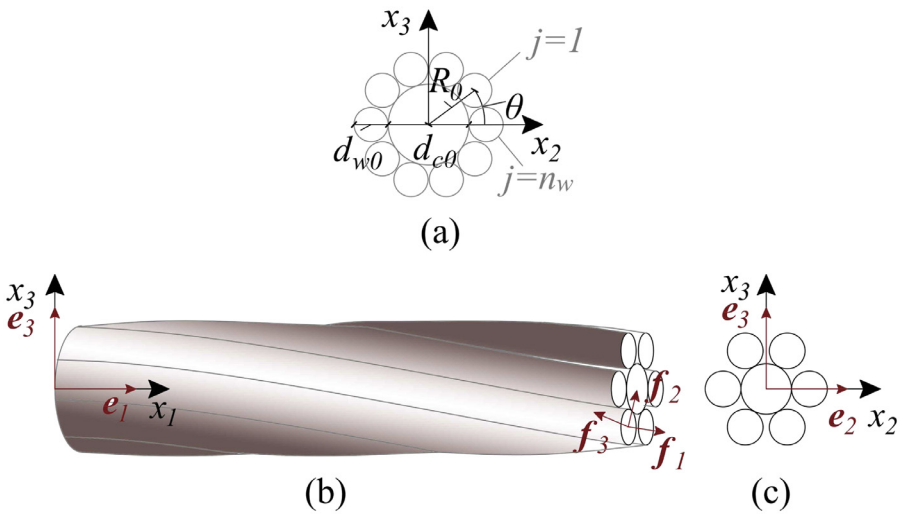

Fig. 1. Geometry of the strand. (a) Cross section of a single-layer strand made of a core wire surrounded by n_w external wires. (b) Side view of a 1/6 strand (i.e. $n_w = 6$). (c) Cross section of a 1/6 strand. The effect of the lay angle on the projection of the cross sections of the wires is neglected in (a) and (c).

and:

$$\tau_0 = \frac{\sin(\alpha_0)\cos(\alpha_0)}{R_0} \tag{5}$$

The geometry of each wire in the reference configuration of the strand, hence, can be completely described, through Eqs. (1)–(5), as a function of the swept angle θ and of two construction parameters among the helix radius R_0, the pitch P_0, the lay angle α_0. Different parameterizations of the wire centerline (Eq. (1)) will be also exploited in this work and can be obtained through a suitable change of coordinates. More in details, by considering an infinitesimal segment of the helix and denoting as S_0 an arc-length coordinate defined on the wire centerline, the following relations can be easily derived:

$$dS_0 \cos(\alpha_0) = dx_1 \tag{6}$$

$$dS_0 \sin(\alpha_0) = R_0 d\theta \tag{7}$$

The equations above can be integrated, along with suitable initial conditions, to obtain the closed-form relations between the coordinates θ, S_0 and x_1.

2.2. Geometrical description of the wire-to-core contact patches

Two types of contact can be basically distinguished within the strand (see e.g. Cardou and Jolicoeur, 1997): the *radial* contact, between the external wires and the core, and the *lateral* (or *circumferential*) contact. In the latter case, the external wires are in contact among them, but not with the core wire.

Once the position and orientation of the cross sections of the external wires are completely characterized through Eqs. (1)–(3), the geometric conditions leading to each contact type can be rigorously investigated by projecting the wire cross sections on a plane normal to the centerline of the strand. This is not, in general, a trivial geometric problem (see e.g. Karathanasopoulos and Angelikopoulos, 2016), but can be greatly simplified by assuming that the projected shape of each wire cross section is elliptical, with the minor semi-axis in radial direction and equal to the wire radius. This is, indeed, a very good approximation for typical values of the core and wire diameters and for values of the lay angle going from zero up to 40° (Cardou and Jolicoeur, 1997), i.e. for the whole range of lay angles adopted in the common manufacturing practice.

By denoting as d_{c0} and d_{w0} the diameter of the core wire and of the external wires (see Fig. 1(a)), respectively, the helix radius of the wires (R_0) can be evaluated as: $R_0 = \frac{1}{2}(d_{c0} + d_{w0})$, for the case of radial contact, and: $R_0 = \frac{d_{w0}}{2}\sqrt{1 + \frac{\tan^2\left(\frac{\pi}{2} - \frac{\pi}{n_w}\right)}{\cos^2(\alpha_0)}}$, for the case of lateral contact (Costello, 1990).

In most practical cases, however, the manufacturers provide gaps between the external wires, to reduce friction forces and the secondary tensile stresses which can be induced by the bending of the strand (Costello, 1990; Feyrer, 2007).

In the present work the focus is on applications of relevant practical interest, hence the interaction between the different components of the strand will be investigated under the assumption of purely radial contact. This hypothesis leads to some constraints on the geometric parameters defined in the reference configuration of the problem, namely: (a) the ratio ξ_0 between the diameter of the external wires and the one of the core should be lower than one, i.e.: $\xi_0 = \frac{d_{w0}}{d_{c0}} < 1$; and (b) the lay angle should be smaller than the maximum value $\alpha_{0,\max}$ corresponding to the onset of lateral contact.

By imposing that the helix radius R_0 satisfies at once the geometric conditions for the radial and lateral contact previously discussed, the value of the angle $\alpha_{0,\max}$ can be easily calculated and the geometric conditions ensuring the radial contact in the reference configuration of the strand can be stated as:

$$\alpha_0 < \alpha_{0,\max} = \arccos\left(\sqrt{\frac{\tan^2\left(\frac{\pi}{2} - \frac{\pi}{n_w}\right)}{\left(1 + \xi_0^{-1}\right)^2 - 1}}\right), \quad \xi_0 = \frac{d_{w0}}{d_{c0}} < 1 \tag{8}$$

3. Axial-torsional mechanical model of the strand

For the case of a strand loaded by an axial force and a torsional moment it is common to assume that the cross sections remain plane (see e.g. Machida and Durelli, 1972). The strand kinematics can hence be described by the axial displacement $u_s(x_1)$ and the torsional rotation $\varphi_s(x_1)$ of the strand cross section.

The generalized strain variables ε_s and χ_s of the strand model correspond to the axial strain and torsional curvature:

$$\varepsilon_s = \frac{du_s}{dx_1} \tag{9}$$

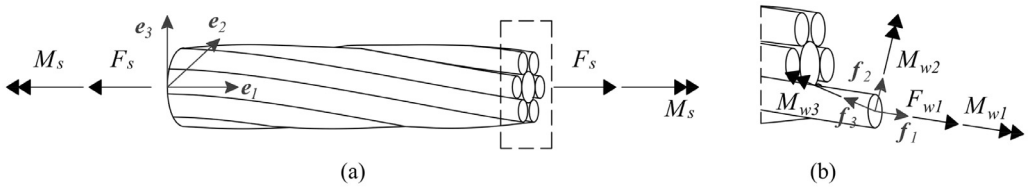

Fig. 2. (a) Straight strand subjected to axial–torsional loads. (b) Generalized stresses on the wire cross section.

$$\chi_s = \frac{d\varphi_s}{dx_1} \tag{10}$$

The work conjugated static quantities are the axial force F_s and torsional moment M_s (see Fig. 2(a)). It can be convenient to collect the generalized strain and stress variables in the column matrices: $\boldsymbol{\varepsilon}_s = (\varepsilon_s,\ \chi_s)^T$, $\boldsymbol{\sigma}_s = (F_s,\ M_s)^T$.

The experimental evidence, briefly recalled in Section 1, shows that the axial-torsional response of the strand under service loading conditions can be well represented by a linear elastic constitutive model. The elastic strain energy per unit of length (dU/dx_1) of the strand can then be written as:

$$\frac{dU}{dx_1} = \frac{1}{2}\boldsymbol{\sigma}_s^T\boldsymbol{\varepsilon}_s = \frac{1}{2}\boldsymbol{\varepsilon}_s^T\mathbf{K}_s\boldsymbol{\varepsilon}_s \tag{11}$$

where $\mathbf{K}_s$ is the stiffness matrix of the strand section. The matrix $\mathbf{K}_s$ which has to be positive definite and symmetric as a consequence of the elasticity assumption, can be defined as:

$$\mathbf{K}_s = \begin{pmatrix} EA & C_T \\ C_T & GJ \end{pmatrix} \tag{12}$$

having denoted with EA and GJ the direct axial and torsional stiffness coefficients, and with C_T the axial-torsional stiffness coupling term.

If derived with a non consistent model, $\mathbf{K}_s$ will be non-symmetric. In contrast to several well known works of the literature (e.g.: Machida and Durelli, 1972; Kumar and Cochran, 1987; Argatov, 2011), which lead to a non-symmetric matrix $\mathbf{K}_s$, in the rest of this work the linear model of Eq. (11) will be derived in a consistent way. A symmetric stiffness matrix is obtained in this paper starting from the individual modeling of the wires as linear elastic curved thin rods (Section 4). The interaction between the external wires and the core wire is modeled as an Hertzian normal contact problem (Section 5), and a comprehensive internal non-linear kinematic model is derived to relate the generalized strains of the wires to the ones of the strand, fully accounting for the contraction of the helix radius of the external wires induced by the loading (Section 6). The kinematic relations are subsequently linearized (Section 7) to express, under the assumptions of small displacements, the strain energy U and to derive the stiffness matrix $\mathbf{K}_s$, leading to remarkably compact equations (Section 8).

4. Mechanical model of the wires

Focusing on single-layer strands, a discrete modeling approach is adopted in this work, based on the formulation firstly proposed by the authors in Foti and Martinelli (2016). Each wire of the strand is described within the framework of the classic Kirchhoff–Clebsch–Love theory (Love, 1944), under the further assumption of small displacements and strains. Accordingly, the generalized stresses of the wire model (see Fig. 2(b)) are defined as the axial force F_{w1}, the torsional moment M_{w1} and the bending moments M_{w2} and M_{w3}, i.e.: the moments acting with respect to the direction of the Serret–Frenet unit vectors $\{\mathbf{f}_k\}$ $(k = 1, 2, 3)$. The work-conjugated strain measures are the axial strain ε_w (i.e. the elongation of the wire centerline), the torsional curvature χ_{w1}, and the bending curvatures χ_{w2} and χ_{w3}.

4.1. Generalized strain variables

The axial strain of the wires can be defined as:

$$\varepsilon_w = \frac{dS}{dS_0} - 1 \tag{13}$$

where dS_0 and dS are the infinitesimal lengths of a wire segment in the reference and deformed configuration, respectively.

The mechanical curvatures of the wires $(\chi_{wk},\ k = 1, 2, 3)$ can be conveniently collected in the column matrix $\boldsymbol{\chi}_w = (\chi_{w1}, \chi_{w2}, \chi_{w3})^T$ and expressed as a function of the rotations of the wire cross sections through the following equation (Huang, 1973; Foti and Martinelli, 2016):

$$\boldsymbol{\chi}_w(S_0) = \frac{d\boldsymbol{\varphi}_w(S_0)}{dS_0} + \boldsymbol{\Omega}_0\boldsymbol{\varphi}_w(S_0) \tag{14}$$

where $\boldsymbol{\varphi}_w = (\varphi_1, \varphi_2, \varphi_3)^T$ is a column matrix storing the rotations of the wire cross section with respect to the directions of the Serret–Frenet unit vectors, while $\boldsymbol{\Omega}_0$ is the skew-symmetric matrix:

$$\boldsymbol{\Omega}_0 = \begin{pmatrix} 0 & -\kappa_0 & 0 \\ \kappa_0 & 0 & -\tau_0 \\ 0 & \tau_0 & 0 \end{pmatrix} \tag{15}$$

4.2. Equilibrium equations

The equilibrium equations can be written in the reference configuration of the wire with the following concise matrix notation (Foti and Martinelli, 2016):

$$\begin{cases} \frac{d\mathbf{F}_w(S_0)}{dS_0} + \boldsymbol{\Omega}_0\mathbf{F}_w(S_0) + \mathbf{p}(S_0) = \mathbf{0} \\ \frac{d\mathbf{M}_w(S_0)}{dS_0} + \boldsymbol{\Omega}_0\mathbf{M}_w(S_0) + \mathbf{i}_1 \times \mathbf{F}_w + \mathbf{m}(S_0) = \mathbf{0} \end{cases} \tag{16}$$

where: $\mathbf{F}_w(S_0)$ and $\mathbf{M}_w(S_0)$ are two column matrices storing, respectively, the cross sectional forces $F_{wk}(S_0)$ and moments $M_{wk}(S_0)$ acting in the direction of the unit vectors of the Serret–Frenet basis $\{\mathbf{f}_k(S_0)\}$ $(k = 1, 2, 3)$; $\mathbf{i}_1$ is the column matrix: $\mathbf{i}_1 = (1, 0, 0)^T$; $\mathbf{p}(S_0)$ and $\mathbf{m}(S_0)$ are two column matrices collecting the components in the direction of the unit vectors $\{\mathbf{f}_k(S_0)\}$, respectively, of a generic system of external forces and couples per unit length of the wire centerline.

It is worth noting that the shear force components $F_{w2}(S_0)$ and $F_{w3}(S_0)$ are not generalized stresses of the model. Hence, whenever needed, they can be evaluated *a posteriori* by solving the equilibrium Eq. (16) once the other terms are known.

4.3. Constitutive law

Focusing on the modeling of metallic strands under typical service loading conditions, the behavior of the wires can be modeled as linearly elastic. By denoting as E and ν, respectively the Young modulus and the Poisson coefficient of the material, the following constitutive equations can be introduced for a wire with circular cross section:

$$F_{w1} = EA_w\varepsilon_w \tag{17}$$

$$M_{w1} = \frac{EI_w}{1+\nu}\chi_{w1} \tag{18}$$

$$M_{w2} = EI_w\chi_{w2} \tag{19}$$

$$M_{w3} = EI_w\chi_{w3} \tag{20}$$

where A_w and I_w are, respectively, the area and second area moment (with respect to a principal axis of inertia) of the wire cross section.

5. The wire-core contact model

As already discussed in Section 2, gaps between the external wires are usually provided by the manufacturers to improve the bending behavior of the strands (see e.g. Costello, 1990; Feyrer, 2007). Starting from this observation, a purely radial contact model between the external wires and the core is developed in this section.

5.1. Equilibrium equations

The contact between an external wire and the core initially takes place along a continuous line on the external surface of the core. On each contact line, a system of normal and tangential contact forces per unit of length can be introduced to describe the interaction between the two bodies. The equilibrium conditions of the wires can then be stated by means of the Eq. (16).

Although general in nature, this approach would lead to a system of six coupled differential equilibrium equations. Further coupling of the equilibrium equations with the local wire-core contact model would then make the searching for analytical solutions of the problem very difficult, if not impossible, naturally calling for the adoption of a numerical solution strategy (e.g. Meng et al., 2016; Chen et al., 2017; Xiang et al., 2017).

A different approach is pursued in this work by noticing that the equilibrium equations of the wire can be greatly simplified by assuming that: (1) the distributed moments due to the offset between the centerline of the wire and the contact line are negligible, (2) the tangential contact forces are parallel to the unit vector tangent to the centerline of the wire and, (3) the effect of the wire shear forces is negligible. The third hypothesis makes the wire translational equilibrium equations decoupled from the rotational ones. Furthermore, the only rotational equation not identically satisfied is the one about the normal direction. The simplifying assumption (3) is only used in the calculation of the normal contact force and, as shown in Appendix A, has a practically negligible effect.

Under the previous assumptions, the indefinite equilibrium equations of the wire, with respect to translations, can be deduced from the simplified scheme depicted in Fig. 3. Indeed, the translational equilibrium equations in the radial and tangential directions (see Eq. (16)) become:

$$\begin{cases} \kappa_0 F_{w1} - \frac{p_n}{\gamma_0} = 0 \\ \frac{dF_{w1}}{dS_0} - \frac{p_t}{\gamma_0} = 0 \end{cases} \tag{21}$$

where: p_n and p_t are, respectively, the normal and tangential contact forces per unit of length; κ_0 is the normal curvature of the wire centerline (see Eq. (4)) and γ_0 is a correction coefficient defined as the ratio between the infinitesimal length of the wire centerline (dS_0) and the one of the contact line (dS_{c0}), i.e.: $\gamma_0 = dS_0/dS_{c0}$. The correction coefficient γ_0 can be easily evaluated as:

$$\gamma_0 = \frac{1+\xi_0}{1+\xi_0\left(1-\sin^2(\alpha_0)\right)} \tag{22}$$

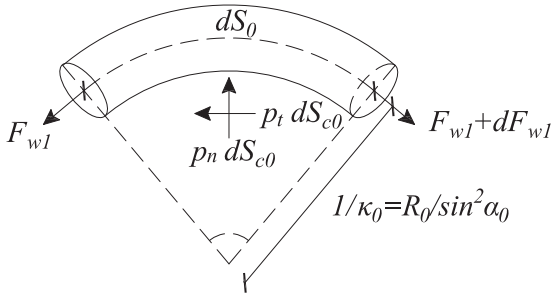

Fig. 3. Equilibrium of the infinitesimal segment dS of an external wire in contact with the core. The symbol dS_{c0} denote the infinitesimal length of the contact line.

Under the hypothesis of excluding rupture of the wires, the internal geometry of the strand is always symmetric with respect to the centerline (axis x_1 in the SRS, see Section 2). The action of a self-equilibrated system of axial forces and torsional moments at the end sections of the strands, hence, leads to an helical-symmetric problem. As a consequence, all the external wires behave identically and are characterized by a constant stress–strain state along their length. In particular, the gradient of the axial force of the wires turns out to be identically equal to zero and from Eq. (21)-b) one simply has: $p_t = 0$. On the other, hand, by solving Eq. (21)-a) with respect to p_n the (constant) normal contact force between the external wires and the core wire can be obtained as:

$$p_n = \gamma_0\kappa_0 F_{w1} \tag{23}$$

Please notice that, in order to satisfy the unilateral radial contact condition all along the wire-core contact line, the contact force p_n must be greater than zero. This implies, through Eq. (23), $F_{w1} > 0$.

The normal contact forces can be expressed as a function of the wire axial strain. By substituting Eqs. (4), (17) and (22) in Eq. (23), the following expression can be obtained:

$$p_n = \frac{EA_w}{R_0}\Gamma_p(\alpha_0,\xi_0)\varepsilon_w \tag{24}$$

where the function $\Gamma_p(\alpha_0,\xi_0) = \frac{(1+\xi_0)\sin^2(\alpha_0)}{1+\xi_0(1-\sin^2(\alpha_0))}$ summarizes the dependence on the lay angle and wire-to-core diameter ratio. Γ_p is practically independent of ξ_0, and can be approximated as $\sin^2(\alpha_0)$ for small values of the lay angle α_0.

5.2. Half-width of the contact strip

The axial force acting in the external wires tends to press them onto the core due to the helicoidal shape of the wires centerline, and the initial contact line is transformed into a contact strip having width $2b$. Clear evidences of this contact mechanism have been provided e.g. by Urchegui et al. (2008) through a detailed inspection of the internal contact surfaces in a metallic stranded rope subjected to a combination of tensile and bending loads.

The wire-core interaction can be modeled as an Hertzian contact problem. By neglecting the inclination of the centerline of the external wire with respect to the one of the core wire, the half-width (b) of the contact strip can be evaluated by means of the classic solution (see e.g.: Roark, 1965; Johnson, 1985) for the contact between two parallel cylinders pressed together by a load per unit length p_n (defined in Eq. (23) or, equivalently, in Eq. (24)):

$$\bar{b} = \sqrt{\frac{2\xi_0\bar{p}_n}{1+\xi_0}} \tag{25}$$

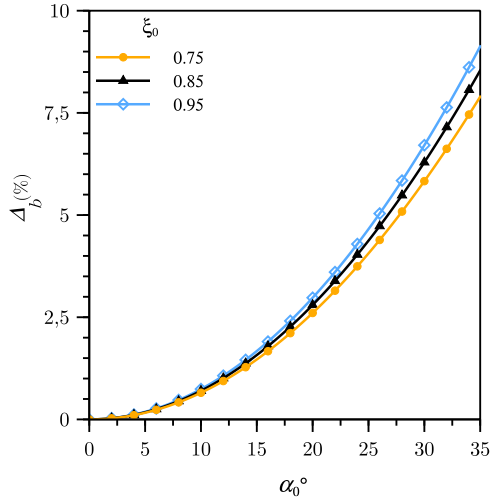

Fig. 4. Comparison between the two different expressions for the evaluation of the half-width of the contact strip reported in Eqs. (25) and (27). The difference between the two expressions is defined as: $\Delta_b = (\bar{b}_\alpha - \bar{b})/\bar{b}$. The results are shown as a function of the lay angle α_0 and for three different values of the wire-core diameter ratio: $\xi_0 = 0.75,\ 0.85,\ 0.95$.

where: $\bar{b} = b/d_{c0}$ and $\bar{p}_n$ is the non-dimensional contact force, here defined for the most common case of mono-metallic strands as:

$$\bar{p}_n = \frac{2\left(1-\nu^2\right)}{\pi E d_{c0}} p_n \tag{26}$$

where E and ν denote, respectively, the Young modulus and the Poisson coefficient of the material. A modified expression for the half-width of the contact strip has been proposed by Argatov (2011) to account for the angle between the centerline of the external and core wire. This can be reported, for comparison purposes, in a non-dimensional form analogous to the previously introduced Eq. (25) as:

$$\bar{b}_\alpha = \sqrt{\frac{2\xi_0 \bar{p}_n}{1+\cos^2(\alpha_0)\xi_0}} \tag{27}$$

A comparison between the results of Eqs. (25) and (27) is shown in Fig. 4 for three different values of the wire-core diameter ratio ($\xi_0 = 0.75,\ 0.85,\ 0.95$). Within the range of practical values herein considered, the difference $\Delta_b = (\bar{b}_\alpha - \bar{b})/\bar{b}$ coming from the two formulae appears comparatively less affected by the value of the wire-core diameter ratio than by the value of the lay angle, being lower than about 2.5% for $\alpha_0 \le 20°$ but rapidly increasing up to values in the range of 7.5–9% (depending on the value of ξ_0) for $\alpha_0 = 35°$. However, given the minor additional computational burden in using Eq. (27), this will be nevertheless retained in the following developments.

5.3. Normal contact compliance

Once the external wires have come in contact with the core wire, their geometry changes. One of the goals of the proposed formulation is to include in a consistent way the effects of this variation in the computation of the strand mechanical response. To this end, a crucial issue is to describe the change in the radius of the helices, which is related to the normal approach δ_n (see Fig. 5) between the centerline of the external wire and the one of the core.

In order to compute the value of δ_n as a function of the contact force p_n a two-dimensional plane strain contact problem has to be considered, leading to a solution which, focusing on mono-metallic

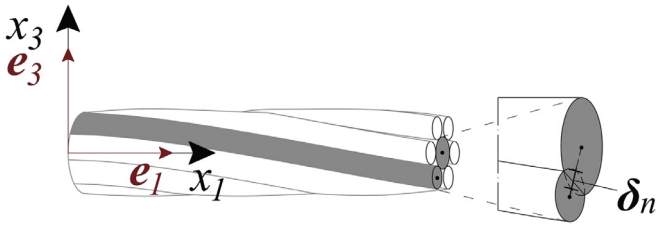

Fig. 5. Schematic representation of the normal approach δ_n between the centerline of the external wire and the one of the core.

strands, can be cast in the following non-dimensional form:

$$\bar{\delta}_n = \left(\ln\left(\frac{\xi_0}{\bar{b}_\alpha^2}\right) + \bar{D}_{bc}\right)\bar{p}_n \tag{28}$$

where $\bar{\delta}_n = \delta_n/d_{c0}$, $\bar{D}_{bc}$ is a non-dimensional constant and $\bar{b}_\alpha$ is the half-width of the contact strip given by Eq. (27). It is worth noticing that neglecting the effect of the lay angle when evaluating the half-width of the contact strip (i.e. using Eq. (25)) leads to practically negligible errors in the equation above. Furthermore, by noticing that Eq. (27) can be rewritten as:

$$\frac{\bar{b}_\alpha^2}{\xi_0} = \frac{2\bar{p}_n}{1+\cos^2(\alpha_0)\xi_0} \tag{29}$$

and by substituting into (28), the non-dimensional normal contact approach can also be expressed, fully highlighting the role of the contact force, as:

$$\bar{\delta}_n = \left(\bar{D}_{bc} + \ln\left(\frac{1+\cos^2(\alpha_0)\xi_0}{2\bar{p}_n}\right)\right)\bar{p}_n \tag{30}$$

The value of the normal approach δ_n depends in general on the contact stresses given by the Hertz theory (near field of the stress distribution), and on the shape, size, loading and boundary conditions of the bodies in contact (far field of the stress distribution), which lead to different values of the constant $\bar{D}_{bc}$. In Fig. 6 are shown two different contact layouts that can be found in the literature on metallic strands. The approach in Fig. 6(a) can be regarded as a classic one and traced back to the works of Starkey and Cress (1959) and Leissa (1959). The same contact layout has been later adopted by several other authors (e.g. Raoof, 1983; Goudreau et al., 1998; Foti et al., 2017). In computing δ_n with this approach, contact takes independently place between each external wire and the central wire, which allows for adopting the approximate solution proposed by Roark (1965) for the contact between two parallel cylinders, i.e.: $\bar{D}_{bc} = 2/3$. This basically corresponds to having neglected the role of all the other external wires in the boundary conditions of the core wire, and will be denoted as Uncoupled Contact Layout (UCL).

In Fig. 6(b) a more refined approach is shown, denoted in following as the Coupled Contact Layout (CCL), in which contact takes place at the same time between all the external wires and the core one (but not between the external wires themselves). This case has been studied by Argatov (2011) through an application of the method of matched asymptotic expansions (Argatov, 2001), leading to a closed form solution, for an even number of external wires, which can be recast as:

$$\bar{D}_{bc} = 1 - \bar{D}_{bc}^{(w)} - \bar{D}_{bc}^{(c)} \tag{31}$$

where the coefficients $\bar{D}_{bc}^{(w)}$ and $\bar{D}_{bc}^{(c)}$ are respectively related to the deformation of the external wire and of the core wire, and can be expressed as:

$$\bar{D}_{bc}^{(w)} = \frac{5-4\nu}{8(1-\nu)} \tag{32}$$

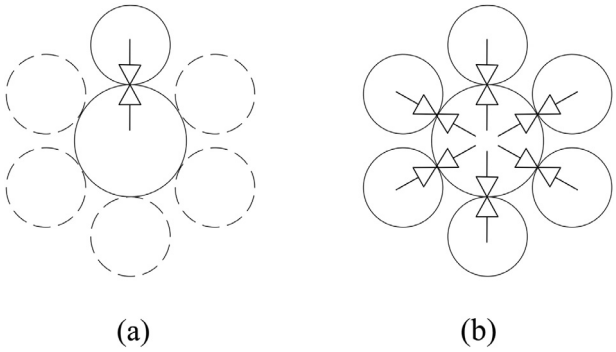

Fig. 6. Schematic representation of: (a) the Uncoupled Contact Layout (UCL), and (b) the Coupled Contact Layout (CCL).

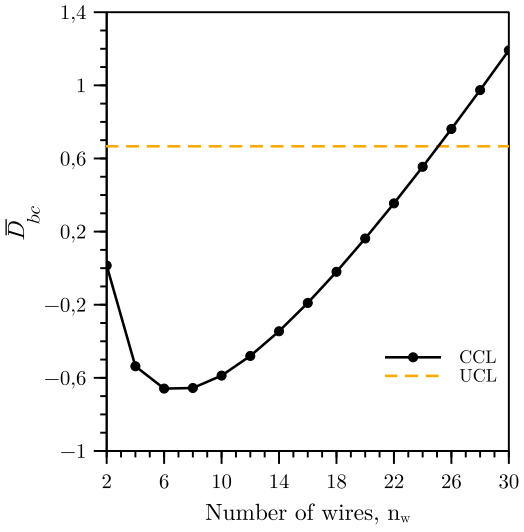

Fig. 7. Comparison between different approaches for the evaluation of the constant $\bar{D}_{bc}$ (see Eq. (28)): Uncoupled Contact Layout (UCL) – schematically depicted in Fig. 6(a), and Coupled Contact Layout (CCL), schematically depicted in Fig. 6(b). The results are shown as a function of the number of external wires of the strand (n_w). Computations have been performed by assuming a Poisson coefficient equal to $\nu = 0.3$.

$$\bar{D}_{bc}^{(c)} = \frac{n_w}{2} - \ln(2) + \sum_{j=1}^{\frac{n_w}{2}-1} \ln\left(\tan\left(\frac{\pi j}{n_w}\right)\right)\cos\left(\frac{2\pi j}{n_w}\right) - \frac{\pi}{4}\frac{(1-2\nu)}{(1-\nu)}\sin\left(\frac{2\pi j}{n_w}\right) \tag{33}$$

In the special case of six external wires ($n_w = 6$), the Eq. (33) above reads:

$$\bar{D}_{bc}^{(c)} = 3 - \ln\left(2\sqrt{3}\right) - \frac{\pi\sqrt{3}}{4}\frac{(1-2\nu)}{(1-\nu)} \tag{34}$$

Fig. 7 compares the value of $\bar{D}_{bc}$ coming from the two examined contact models for a Poisson coefficient equal to $\nu = 0.3$. Positive values of $\bar{D}_{bc}$ are related to a reduction of the distance between the center of the external wire and the core one. In the first contact model there will always be a reduction of such distance, since the deformation effects related to the Young modulus and the Poisson coefficient are not in competition. This is due to the fact that the far field solution disregards the possibility of having several external wires in contact with the central wire at the same time. Instead, the more refined model developed by Argatov (2011) predicts almost a null contribution in the case of two external wires in contact with the core wire, an increment of the distance between the center of the external wire and the core one for all practical numbers of external wires, and a reduction of the distance for an unrealistically large number of external wires.

To the authors' knowledge there is in the literature no direct comparison of the effect coming from having adopted one or the other of the contact layouts previously described. Thanks to the modularity of the formulation to model the mechanical response of metallic strands we propose in this work, leaving all the other aspects the same, it will be possible a direct and fair comparison.

The normal contact compliance can be easily evaluated as the derivative of the total normal approach with respect to the normal contact force per unit length (see e.g. Johnson, 1985), i.e.:

$$C_n(p_n) = \frac{d\delta_n}{dp_n} = \frac{2\left(1-\nu^2\right)}{\pi E}\bar{C}_n(\bar{p}_n) \tag{35}$$

where $\bar{C}_n(\bar{p}_n)$ is the non-dimensional normal contact compliance that can be evaluated from Eq. (30):

$$\bar{C}_n(\bar{p}_n) = \frac{d\bar{\delta}_n}{d\bar{p}_n} = \bar{D}_{bc} - 1 - \ln\left(\frac{2\bar{p}_n}{1+\cos^2(\alpha_0)\xi_0}\right) \tag{36}$$

It is worth noting that the non-dimensional normal contact compliance is weakly singular for $\bar{p}_n \to 0$ and a reference value of $\bar{C}_n$ in the reference configuration, that will be denoted as $\bar{C}_{n0}$, has to be assumed as a model parameter. This is important in comparing results of different (both analytical and numerical) models. A possible way to circumvent the weak singularity problem is to calculate $\bar{C}_{n0}$ on the base of a nominal (small) value of the wires axial strain.

For real strands the singularity of $\bar{C}_{n0}$ is not a problem since due to residual formation stresses there will never be zero contact force in the reference configuration (Rawlins, 2005; Frigerio et al., 2016). From consideration of the residual stresses related to the formation of the strand (Rawlins, 2005), $\bar{C}_{n0}$ turns out to be approximately in the range: $7 \le \bar{C}_{n0} \le 14$ for lay angles in the range $5^\circ \le \alpha_0 \le 20^\circ$.

6. Internal kinematics of the strand

Axial-torsional loading of a straight strand can be defined as a "geometry preserving" loading case (Leech, 2002). Due to the helical symmetry with respect to the strand centerline, it can indeed be shown (see e.g. Costello, 1990) that: (1) the core remains straight and is subjected to the same axial strain and torsional curvature of the strand; (2) the centerline of the external wires is transformed into a circular helix with, in general, a different radius, R, and lay angle, α, with respect to the ones of the reference configuration (i.e. R_0 and α_0). Furthermore, all external wires are subjected to the same stress–strain state, which is also constant along their length.

The *radial contraction parameter* will be defined in the following as the ratio between the values of the helix radius in the deformed (R) and reference (R_0) configuration:

$$\beta = \frac{R}{R_0} = 1 + \frac{\Delta R}{R_0} \tag{37}$$

where $\Delta R = R - R_0$ is the variation of the helix radius of the external wires with respect to the reference configuration. Under the action of a tensile load applied to the strand, the helix radius tends to decrease, giving $\Delta R \le 0$ and $\beta \le 1$.

6.1. Axial strains of the wires

The axial strain of the core wire (ε_c) can be simply defined as:

$$\varepsilon_c = \varepsilon_s \tag{38}$$

The axial strain of an external wire (ε_w) can be evaluated, following (Knapp, 1979), by considering the ratio between the developed length of an infinitesimal segment of its centerline before (dS_0) and after (dS) the deformation of the strand: $\frac{dS}{dS_0} = \varepsilon_w + 1 = \frac{\cos(\alpha_0)}{\cos(\alpha)}(1+\varepsilon_s)$, where α and α_0 are the lay angles in the deformed and reference configuration, respectively (see also Section 2). Geometric considerations (see Knapp, 1979) lead then to $\cos(\alpha) = (1+\varepsilon_s)/(\sqrt{(1+\varepsilon_s)^2 + \beta^2\tan^2(\alpha_0)(1+R_0\chi_s/\tan(\alpha_0))^2})$, where β is the radial contraction parameter defined in Eq. (37). Finally, with the notation used in this work the kinematic relation proposed by Knapp can be rewritten as:

$$\varepsilon_w = \sqrt{\cos^2(\alpha_0)(1+\varepsilon_s)^2 + \beta^2\sin^2(\alpha_0)\left(1+\frac{R_0\chi_s}{\tan(\alpha_0)}\right)^2} - 1 \tag{39}$$

6.2. Mechanical curvatures of the wires

By assuming that the cross sections of the wires rigidly follow the rotation of the strand cross section, the mechanical curvatures of the external wires can be evaluated, starting from Eq. (14), by exploiting the approach firstly proposed by Foti and Martinelli (2016). For the case of constant torsional curvature of the strand (see also Foti and de Luca, 2016), the following expressions can be easily obtained (calculations are fully reported in the Appendix B):

$$\chi_{w1} = \cos^2(\alpha_0)\chi_s \tag{40}$$

$$\chi_{w2} = 0 \tag{41}$$

$$\chi_{w3} = \sin(\alpha_0)\cos(\alpha_0)\chi_s \tag{42}$$

Those of the core wire (χ_{c1}, χ_{c2}, χ_{c3}) can be simply obtained from Eqs. (40)–(42) for $\alpha_0 = 0$:

$$\chi_{c1} = \chi_s \tag{43}$$

$$\chi_{c2} = \chi_{c3} = 0 \tag{44}$$

6.3. Variation of the helix radius

The total variation ΔR of the helix radius of the external wires of the strand can be decomposed as the sum of ΔR_ν, which is the contribution accounting for the contraction of the diameters of the core and of the external wires due to the Poisson's effect, and ΔR_f, which is the contribution accounting for the radial deformation of the wire-core contact surfaces (also called *flattening*):

$$\Delta R = \Delta R_\nu + \Delta R_f \tag{45}$$

The linear decomposition assumption leads to a great simplification in the statement of the mechanical problem, while introducing practically negligible approximations. The accuracy of this approximation can be checked *a posteriori* through comparisons with both experimental data and numerical results obtained from more refined modeling approaches, e.g. FE models (see Section 9).

By substituting Eq. (45) into Eq. (37) the radial contraction parameter β becomes:

$$\beta = 1 + \frac{\Delta R_\nu}{R_0} + \frac{\Delta R_f}{R_0} = \beta_\nu + \beta_f - 1 \tag{46}$$

where the Poisson and flattening related parts of the radial contraction parameter have been respectively defined as:

$$\beta_\nu = 1 + \frac{\Delta R_\nu}{R_0} \tag{47}$$

$$\beta_f = 1 + \frac{\Delta R_f}{R_0} \tag{48}$$

In the following, each physical mechanism contributing to the total variation of the helix radius will be individually considered.

6.3.1. Poisson effect

By recalling the meaning of ε_c, ε_w, d_{c0} and d_{w0}, the change in the helix radius due to the Poisson's effect can be expressed, for a mono-metallic strand, as:

$$\Delta R_\nu = -\frac{\nu}{2}(\varepsilon_c d_{c0} + \varepsilon_w d_{w0}) \tag{49}$$

where ν is the Poisson coefficient of the material.

By recalling that $\xi_0 = \frac{d_{w0}}{d_{c0}}$ and $\frac{d_{c0}}{2R_0} = \frac{1}{1+\xi_0}$ (see Section 2), by substituting Eq. (49) in the definition of the radial contraction parameter β_ν (Eq. (47)), the following expression can be obtained:

$$\beta_\nu = 1 - \frac{\nu}{1+\xi_0}(\varepsilon_c + \xi_0\varepsilon_w) \tag{50}$$

6.3.2. Flattening effect

By recalling the definition introduced in Section 5.3 for the non-dimensional normal contact approach $\bar{\delta}_n$ between the external wires and the core wire, the change in the helix radius of the external wires due to the flattening of the contact surfaces can be expressed as:

$$\Delta R_f = -\bar{\delta}_n d_{c0} \tag{51}$$

and by substituting Eq. (51) in (48), the radial contraction parameter β_f becomes:

$$\beta_f = 1 - \frac{2\bar{\delta}_n}{1+\xi_0} \tag{52}$$

7. Linearized internal kinematic model

In this section, a linearized form of the internal kinematics of the strand is sought, taking into consideration all the assumed physical mechanisms leading to a contraction of the helix radius of the external wires.

It can be noted that the relation in Eq. (39) between ε_w and the components ε_s, χ_s of the generalized strain of strand is non-linear. A classic linearized solution for ε_w (e.g. Machida and Durelli, 1972; Lanteigne, 1985; Foti and Martinelli, 2016), that will be also used in the following for comparison purposes, can be obtained by neglecting the contraction of the helix radius (i.e. $\beta = 1$), and by assuming that ε_s and χ_s are small (i.e. $\varepsilon_s << 1$ and $R_0\chi_s << 1$). Under these assumptions, the linearization of Eq. (39) leads to:

$$\varepsilon_w = \cos^2(\alpha_0)\varepsilon_s + \sin(\alpha_0)\cos(\alpha_0)R_0\chi_s \tag{53}$$

However, β itself does depend non-linearly on ε_w, making the correct linearized solution different from what is currently available in the literature.

Recalling that $\varepsilon_c = \varepsilon_s$, the terms β_ν and β_f, which define β, are two functions of ε_s and ε_w. More in details, β_f is a non-linear function of ε_w while β_ν is a linear function of both ε_s and ε_w. Hence, from Eq. (46), the following general expression can be introduced:

$$\beta = \mathcal{B}(\varepsilon_s, \varepsilon_w) \tag{54}$$

while Eq. (39) becomes:

$$\varepsilon_w = \sqrt{\cos^2(\alpha_0)(1+\varepsilon_s)^2 + \mathcal{B}^2(\varepsilon_s,\varepsilon_w)\sin^2(\alpha_0)\left(1+\frac{R_0\chi_s}{\tan(\alpha_0)}\right)^2} - 1 \tag{55}$$

Eq. (55), which defines the non-linear function $\varepsilon_w = \varepsilon_w(\varepsilon_s, \chi_s)$ in implicit form, can be linearized by resorting to Dini's theorem on implicit functions (see e.g. Dontchev and Rockafellar, 2014). Its expansion in Taylor's series truncated at the first order, reads:

$$\varepsilon_w = A\varepsilon_s + B\chi_s \tag{56}$$

where the coefficients A and B, which are respectively the partial derivative of ε_w with respect to ε_s and χ_s evaluated in the reference configuration (i.e. $\varepsilon_s = 0$ and $\chi_s = 0$) are computed in Appendix C. The resulting expressions are:

$$A = \frac{\cos^2(\alpha_0) - \frac{\nu \sin^2(\alpha_0)}{1+\xi_0}}{1 + \frac{\nu\xi_0 \sin^2(\alpha_0)}{1+\xi_0} + \frac{2(1-\nu^2)\xi_0^2 \bar{C}_{n0} \sin^4(\alpha_0)}{(1+\xi_0)(1+\xi_0(1-\sin^2(\alpha_0)))}} \tag{57}$$

$$B = \frac{\sin(\alpha_0)\cos(\alpha_0)R_0}{1 + \frac{\nu\xi_0 \sin^2(\alpha_0)}{1+\xi_0} + \frac{2(1-\nu^2)\xi_0^2 \bar{C}_{n0} \sin^4(\alpha_0)}{(1+\xi_0)(1+\xi_0(1-\sin^2(\alpha_0)))}} \tag{58}$$

The coefficient $\bar{C}_{n0}$, which is the value of the non-dimensional normal contact compliance in the reference configuration, can be considered as a parameter of the model proposed, and calculated as explained in Section 5.3.

In terms of classic models for the strand theory, the proposed formulation can recover the simpler formulation of Eq. (53) by dropping the contribution of the Poisson effect (i.e. by assuming $\nu = 0$) and the contribution of the contact compliance (i.e. by assuming $\bar{C}_{n0} = 0$) in the Eqs. (57) and (58) above. This gives: $A = \cos^2(\alpha_0)$, and: $B = \sin(\alpha_0)\cos(\alpha_0)R_0$. The terms A and B, instead, cannot be directly compared with another well known model that includes the effects of the normal contact compliance (Argatov, 2011) since that Author doesn't provide a truly linear expression for ε_w.

It is also worth noticing that, based on the above computations, it is possible to define a linearized expression for the radial contraction parameter:

$$\beta = 1 + C\varepsilon_s + D\chi_s \tag{59}$$

where the constant C and D are given in Appendix C.

Finally, it is worth noticing that the linearized expression $\varepsilon_w = \varepsilon_w(\varepsilon_s, \chi_s)$ of Eq. (56) that we propose is not only valid around the reference configuration of the mechanical problem but, as it will be clear from the comparison with experimental and numerical results (Section 9), has actually a much wider range of validity.

8. Evaluation of the axial-torsional stiffness matrix of the strand

The cross sectional stiffness of the strand can be conveniently evaluated through a classic energetic approach, starting from the expression of the elastic strain energy per unit of length of the strand. This can be evaluated by adding the contributions of the core and of the external wires, i.e.:

$$\frac{dU}{dx_1} = \frac{dU_c}{dx_1} + n_w \frac{dS_0}{dx_1}\frac{dU_w}{dS_0} \tag{60}$$

where U_c and U_w denote, respectively, the elastic strain energy of the core and of a single external wire, while the term dS_0/dx_1 can be calculated from Eq. (6) as: $\frac{dS_0}{dx_1} = \frac{1}{\cos(\alpha_0)}$.

The core strain elastic energy can be computed, by recalling that the core is subjected to the same axial strain ($\varepsilon_c = \varepsilon_s$) and torsional curvature ($\chi_s = \chi_w$) of the strand, as:

$$\frac{dU_c}{dx_1} = \frac{1}{2}EA_c\varepsilon_s^2 + \frac{1}{2}\frac{EI_c}{1+\nu}\chi_s^2 \tag{61}$$

where EA_c and $\frac{EI_c}{1+\nu}$ are, respectively, the axial and torsional stiffness of the core cross section.

The strain energy per unit length of an external wire can be computed by recalling that it is subjected, in general, to a combination of stretch (ε_w), torsion (χ_{w1}) and bending (χ_{w3}):

$$\frac{dU_w}{dS_0} = \frac{1}{2}EA_w\varepsilon_w^2 + \frac{1}{2}\frac{EI_w}{1+\nu}\chi_{w1}^2 + \frac{1}{2}EI_w\chi_{w3}^2 \tag{62}$$

where EA_w, $\frac{EI_w}{1+\nu}$ and EI_w are, respectively, the axial, torsional and bending stiffness of the wire cross section. By substituting Eqs. (56), (40) and (42) in Eq. (62) the strain energy per unit length of the external wire can also be re-written as:

$$\begin{aligned}\frac{dU_w}{dS_0} = {} & \frac{1}{2}EA_wA^2\varepsilon_s^2 + \frac{1}{2}2EA_wAB\varepsilon_s\chi_s \\ & + \left(EA_wB^2 + \cos^4(\alpha_0)\frac{EI_w}{1+\nu} + \sin^2(\alpha_0)\cos^2(\alpha_0)EI_w\right)\chi_s^2\end{aligned} \tag{63}$$

Finally, by comparing Eq. (60) after having substituted Eqs. (61) and (63), with Eq. (11) the strand cross sectional stiffness terms can be defined as:

$$EA = EA_c + \frac{n_wEA_wA^2}{\cos(\alpha_0)} \tag{64}$$

$$C_T = \frac{n_wEA_wAB}{\cos(\alpha_0)} \tag{65}$$

$$\begin{aligned}GJ = {} & \frac{EI_c}{1+\nu} + \frac{\cos^3(\alpha_0)n_wEI_w}{1+\nu} + \cos(\alpha_0)\sin^2(\alpha_0)n_wEI_w \\ & + \frac{n_wEA_wB^2}{\cos(\alpha_0)}\end{aligned} \tag{66}$$

By dropping the contribution of the Poisson effect (i.e. by assuming $\nu = 0$) and the contribution of the contact compliance (i.e. by assuming $\bar{C}_{n0} = 0$) in the evaluation of the coefficient A and B, the stiffness terms already given by Foti and Martinelli (2016) are obtained as a special case from Eqs. (64) to (66).

9. Applications

In the following, the model developed in this work is applied to the study of the axial-torsional response of 1/6 strands. The first example includes comparisons with experimental results and a finite element (FE) solution from the literature. The second example includes details about the mechanics of the local contact between the core and the wires. The third and fourth examples compare the results of the proposed model to those of other researchers for the parametric analysis of a 1/6 wires strand at the variation of the lay angle α_0. The results allow to highlight the range of lay angles in which the hypotheses on the contact model became essentials.

9.1. Example 1

The proposed mechanical model is herein applied to simulate the axial-torsional response of a well documented single-layer steel strand, already studied by several authors, with both analytical and numerical techniques (see e.g.: Jiang et al., 1999; Judge et al., 2012; Yu et al., 2014; Foti and Martinelli, 2016; Foti and de Luca, 2016; Karathanasopoulos et al., 2017). For the same strand, experimental data are reported in Jiang et al. (1999) based on previous works by Utting (1984) and Utting and Jones (1985). The experimental data were obtained by means of a tension-torsion machine fully described in Utting and Jones (1985, 1987a). During the original testing, the strand was subjected in the straight configuration to a combination of axial force and torsional moment applied at the end sections. To this aim the machine applies a prescribed axial elongation to the strand, while the

Table 1
Comparison among theoretical and experimental values of the response parameters: $k_1 = \frac{F_s}{\varepsilon_s}$ and $k_2 = \frac{F_s}{M_s}$. Experimental data are from Jiang et al. (1999). Finite Element (FE) model results are from Foti and de Luca (2016). The results of the proposed analytical formulation have been calculated under several different modeling assumptions and are listed in columns (iv)–(vii). Col. (iv): Coupled Contact Layout ("CCL"), $\nu = 0.30$, $\bar{C}_{n0} = 9.27$. Col. (v): Uncoupled Contact Layout ("UCL"), $\nu = 0.30$, $\bar{C}_{n0} = 10.6$. Col. (vi) Model accounting only for the radial contraction due to the Poisson's effect ("Poisson"), $\nu = 0.30$, $\bar{C}_{n0} = 0$. (vii) Model disregarding for both Poisson and flattening effects on the radial contraction ("Rigid"), $\nu = 0$, $\bar{C}_{n0} = 0$.

	Experimental	FE model	Prop. model (CCL)	Prop. model (UCL)	Prop. model (Poisson)	Prop. model (Rigid)
Fixed-end						
$k_1 = \frac{F_s}{\varepsilon_s} = EA$ (kN)	13,539	13,017	13,402	13,380	13,560	13,853
Difference (%)	–	3.86	1.01	1.18	0.155	2.32
$k_2 = \frac{F_s}{M_s} = \frac{EA}{C_T}$ (1/mm)	1.530	1.526	1.496	1.496	1.492	1.496
Difference %	–	0.261	2.25	2.22	0.248	0.222
Free-end						
$k_1 = \frac{F_s}{\varepsilon_s} = EA - \frac{C_T^2}{GJ}$ (kN)	9140	8775	9200	9192	9261	9409
Difference (%)	–	3.99	0.660	0.566	1.32	2.94

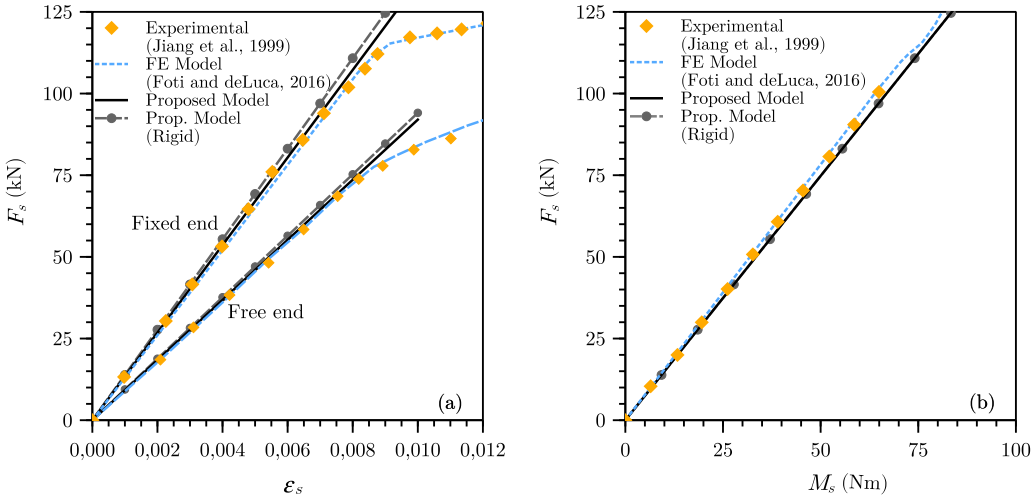

Fig. 8. Comparison among theoretical and experimental results. (a) Axial force (F_s) vs. axial strain (ε_s) of the strand. (b) Axial force (F_s) vs. Torsional moment (M_s) of the strand (fixed-end test). Experimental data as reported in Jiang et al. (1999). Finite Element (FE) model results are from Foti and de Luca (2016).

corresponding axial force is recorded. One end of the strand is fully clamped, while the other can be free (free-end case) or fully restrained (fixed-end case). In the latter case, the reacting torsional moment was recorded. This is a standard experimental setup for tensile testing of metallic strands (see also, e.g., Elata et al., 2004; Feyrer, 2007) since it allows to reproduce the theoretical condition of uniform stress–strain state along the element and provides a quantitative assessment of the axial-torsional coupling. The geometrical parameters of the undeformed strand are: $d_{c0} = 3.94$ mm, $d_{w0} = 3.73$ mm ($\xi_0 = \frac{d_{w0}}{d_{c0}} = 0.947$), $\alpha_0 = 11.8°$. The mechanical parameters are: Young modulus $E = 188$ GPa, Poisson coefficient $\nu = 0.30$.

Fig. 8 shows a comparison of the results obtained with the analytical model presented in this paper and the FE model developed in Foti and de Luca (2016), supplemented with the experimental data as reported in Jiang et al. (1999). Fig. 8(a) shows the relation between the axial force and the axial strain of the strand, Fig. 8(b) the relation between the axial force and torsional moment at the strand ends for the "Fixed end" case. The FE simulations have been performed in ANSYS with a 500 mm stretch of strand, corresponding to about 5 times the lay length of the external wires. The adopted mesh uses 28,000 solid 20 nodes brick elements, with quadratic displacement behavior, and 137,400 nodes. The maximum size of the elements was set equal to 1/5 of the wire diameter in radial direction and 1/40 of the lay length in the longitudinal direction. Further details on the finite element model and solution, including the wire-core contact model, can be found in Foti and de Luca (2016).

The results of the proposed formulation have been computed with a reference value of the non-dimensional normal contact compliance $\bar{C}_{n0} = 9.27$, which corresponds to having assumed in Eqs. (24) and (36) a nominal value of the wire axial strain equal to $\varepsilon_w = 1 \cdot 10^{-3}$ (i.e. about 1/10 of the first yielding strain for typical steel wires) and having computed $\bar{D}_{bc}$ with the CCL approach. For comparison purposes also the results of a rigid contact case, obtained by neglecting both the Poisson and flattening effect (i.e. by assuming $\nu = 0$, $\bar{C}_{n0} = 0$), have been reported as the "Prop. Model (Rigid)" curve. It is worth noting that this special case corresponds to the formulation already presented in Foti and Martinelli (2016).

Excellent agreement is found in the whole linear range of the response between the proposed model and the experimental results and FE simulations for both boundary conditions here considered (free-end and fixed-end). In particular, it is worth noting how the analytical models are able to capture all the essential features of the axial load-strain curve (see Fig. 8(a)) and of the coupling between the axial force and the torsional moment (see Fig. 8(b)) with the same order of accuracy of the more computational demanding FE model. The rigid contact case is not very far away from the other analytical model, consistently with the value of the lay angle being in a range for which the theoretical developments predict similar responses irrespective of the contact model adopted. This aspect will be further investigated in the Examples 3 and 4.

The results from the proposed models are also very close to those of other authors (e.g. the FE models by Jiang et al. (1999) and the more recent ones by Judge et al. (2012), Yu et al. (2014) and Karathanasopoulos et al. (2017)).

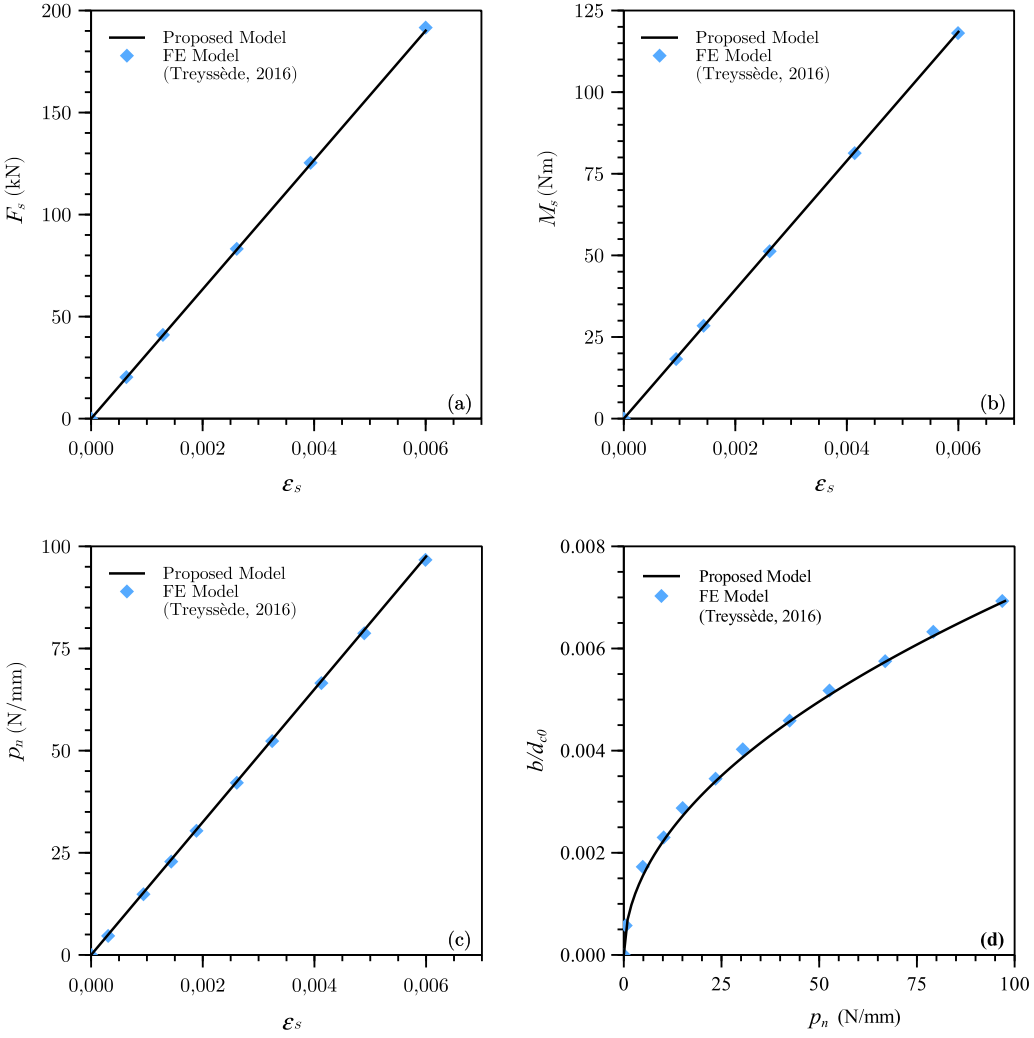

Fig. 9. Comparison among analytical (Proposed model) and FE results (from Treyssède, 2016). (a) Axial force (F_s) vs. axial strain (ε_s) of the strand. (b) Torsional moment (M_s) vs. axial strain (ε_s) of the strand. (c) Normal contact force p_n per unit of length versus axial strain of the strand (ε_s). (d) Non-dimensional half-width of the contact strip (b/d_{c0}) versus p_n.

Since the proposed model is based on the hypothesis of linear elastic material behavior, it is hence unable to reproduce the plastic phenomena which precede the breaking of the strand. Material non-linearity, however, could be easily introduced in the present analytical formulation following what presented in Foti and de Luca (2016).

For the same strand, the values of the response parameter $k_1 = \frac{F_s}{\varepsilon_s}$, $k_2 = \frac{F_s}{M_s}$, which are related to the elastic stiffness, have been listed in Table 1 for the two torsional boundary conditions investigated (i.e. the free- and fixed-end cases). The experimental and FE values have been obtained from the initial slope of the response curves in (Fig. 8(a) and (b)), while the ones of the proposed analytical model have been evaluated through the closed-form expressions presented in the previous Section. To highlight the modularity of the proposed formulation, and to study the implications of the different modeling assumptions, the outcomes obtained considering the CCL contact model ("CCL"), the UCL model ("UCL"), the effect of the radial contraction due to Poisson effect only ("Poisson") and the rigid contact ("Rigid") have been added in Table 1. It can be observed how the discrepancies between the proposed model and the experimental results are always less than 3%, while the relative error on k_1 for the FE model results is always slightly larger.

A deeper insight about the importance of the different radial contraction terms can be gained by computing the value of the cross sectional stiffness coefficients from the data in Table 1. The results are listed in Table 2. As expected, the value of the direct and cross terms of the section stiffness matrix decrease moving from the assumption of a rigid model to one that includes both Poisson and the flattening contraction terms (UCL and CCL). The assumed contact layouts (UCL or CCL) has a minor impact on the strand response for this special strand geometry. The theoretical models give a very accurate prediction of the axial stiffness and of the axial-torsional coupling term, while they all appear too stiff with respect to torsion (with a 7–8% overestimation of the GJ term). The FE model, by contrast, shows a similar accuracy (in the order of 3–4%) in predicting all the stiffness terms.

9.2. Example 2

The accuracy of the local contact model is assessed by comparing the output of the proposed analytical formulation with the results of the FE model recently presented by Treyssède (2016). The numerical experiments simulate a fixed-end tensile test (i.e.: the torsional rotation of the end-sections of the strand is restrained) on a metallic strand having the following geometric and

Table 2
Comparison among theoretical and experimental values of the cross sectional stiffness terms. Experimental data are from Jiang et al. (1999). Finite Element (FE) model results are from Foti and de Luca (2016). The results of the proposed analytical formulation have been calculated under several different modeling assumptions and are listed in columns (iv)–(vii). Col. (iv): Coupled Contact Layout ("CCL"), $\nu = 0.30$, $\bar{C}_{n0} = 9.27$. Col. (v): Uncoupled Contact Layout ("UCL"), $\nu = 0.30$, $\bar{C}_{n0} = 10.6$. Col. (vi) Model accounting only for the radial contraction due to the Poisson's effect ("Poisson"), $\nu = 0.30$, $\bar{C}_{n0} = 0$. (vii) Model disregarding for both Poisson and flattening effects on the radial contraction ("Rigid"), $\nu = 0$, $\bar{C}_{n0} = 0$.

	Experimental	FE model	Prop. model (CCL)	Prop. model (UCL)	Prop. model (Poisson)	Prop. model (Rigid)
EA (kN)	13,539	13,017	13,402	13,380	13,560	13,853
Difference (%)	–	3.86	1.01	1.18	0.155	2.32
C_T (kN m)	8.85	8.53	8.96	8.94	9.09	9.26
Difference %	–	3.60	1.27	1.07	2.71	4.67
GJ (Nm^2)	17.8	17.2	19.1	19.1	19.2	19.3
Difference (%)	–	3.64	7.37	7.28	7.94	8.45

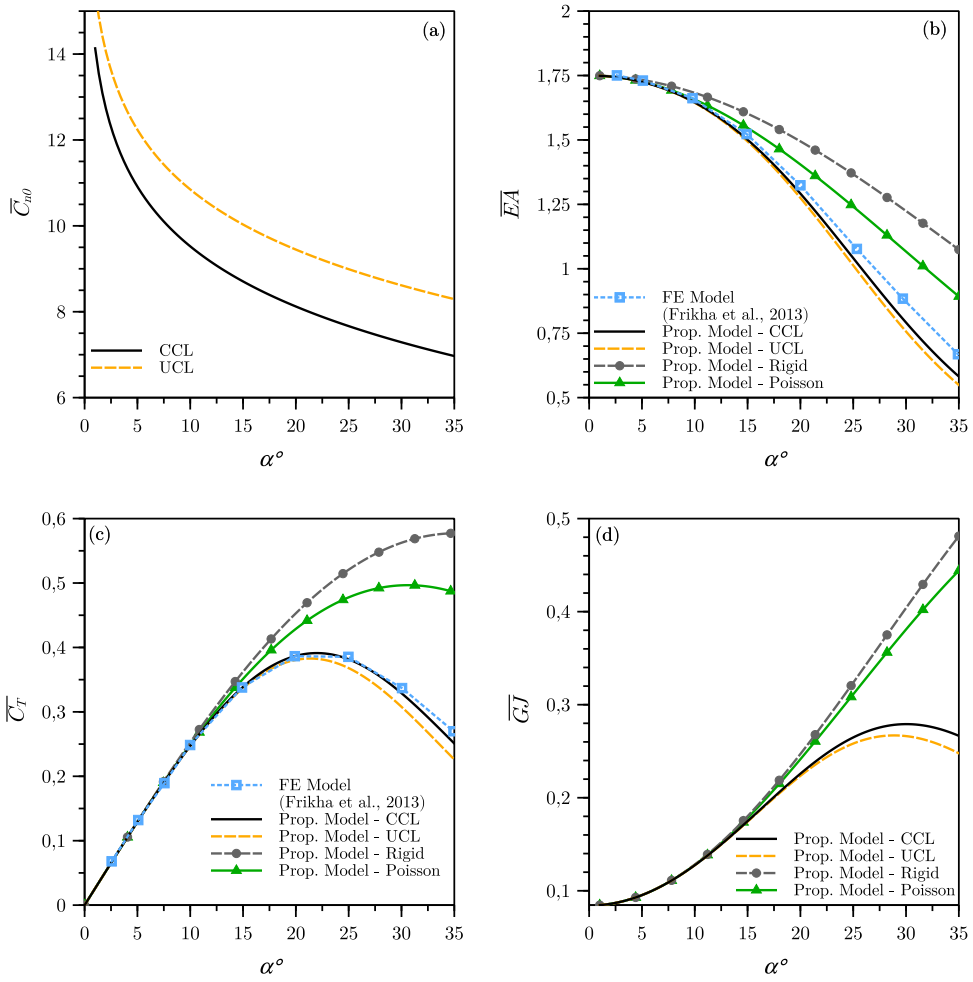

Fig. 10. (a) Non-dimensional contact compliance $\bar{C}_{n0}$ as a function of the lay angle α_0. Results are shown for both the Uncoupled Contact Layout (UCL) and the Coupled Contact Layout (CCL). (b)–(d) Non-dimensional stiffness coefficients as a function of the lay angle α_0. The analytical results of the proposed model (Prop. model CCL, UCL, Poisson and Rigid) are compared to the available FE results from Frikha et al. (2013).

mechanical properties: $d_{c0} = 5.4$ mm, $d_{w0} = 5.22$ mm ($\xi_0 = \frac{d_{w0}}{d_{c0}} = 0.967$); $\alpha_0 = 7.9°$; $E = 217$ GPa; $\nu = 0.28$. The finite element model used a refined triangular finite element mesh to simulate the core to wires contact, comprising 46,893 degrees-of-freedom over the strand cross section.

The value of the non-dimensional normal contact compliance ($\bar{C}_{n0}$) is evaluated by considering a nominal value of the wire axial strain equal to $6 \cdot 10^{-4}$, which corresponds to 1/10 of the maximum strain in the test. The value $\bar{C}_{n0} = 11.9$ is given following the UCL approach ($\bar{D}_{bc} = 2/3$), while a value $\bar{C}_{n0} = 10.6$ is given by the CCL approach ($\bar{D}_{bc} = -0.60$).

Fig. 9(a) shows the relation between the axial force and the strand axial strain ε_s, while Fig. 9(b) that of the torsional moment at the strand ends. Fig. 9(c) reports the normal contact force p_n per unit of length versus the strand axial strain, while Fig. 9(d) the half-width of the contact strip versus p_n. Only the results coming from the more refined CCL contact model with Poisson effects ($\nu = 0.28$, $\bar{C}_{n0} = 10.6$) are reported since

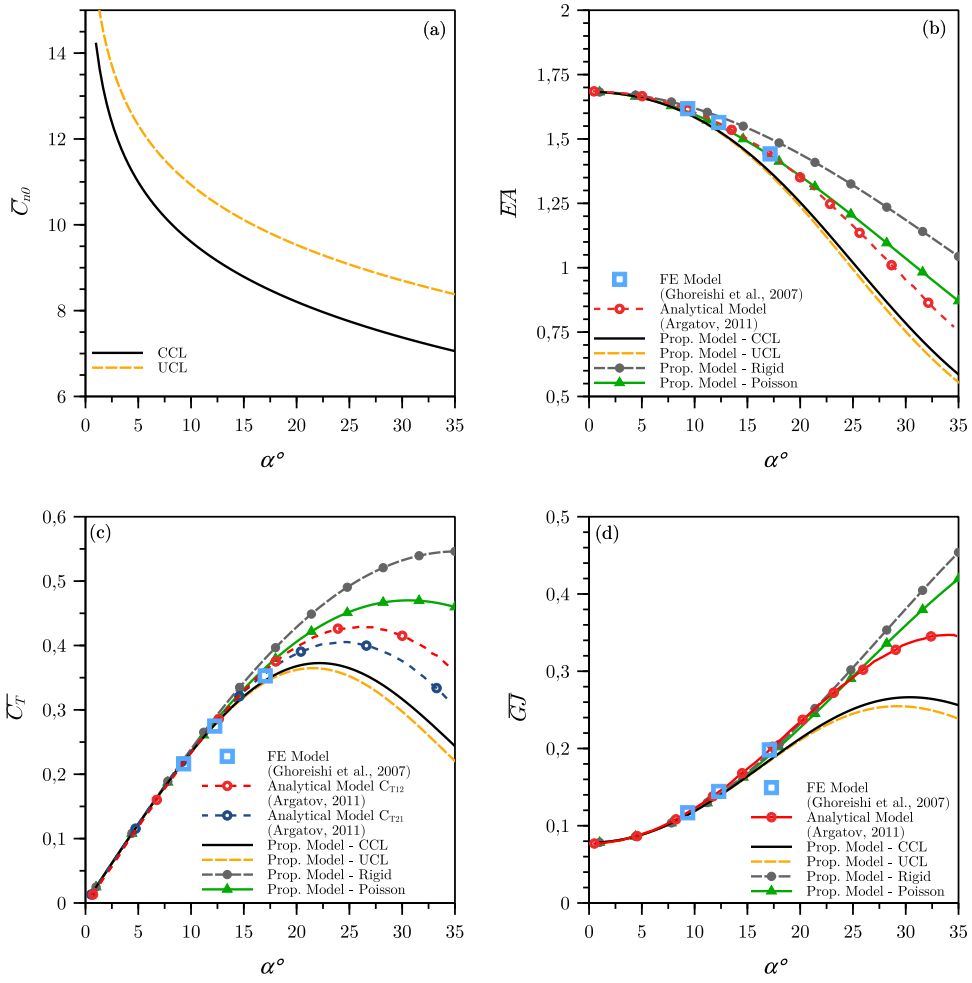

Fig. 11. (a) Non-dimensional contact compliance $\bar{C}_{n0}$ as a function of the lay angle α_0. Results are shown for both the Uncoupled Contact Layout (UCL) and the Coupled Contact Layout (CCL). (b)–(d) Non-dimensional stiffness coefficients as a function of the lay angle α_0. The analytical results of the proposed model (Prop. model CCL, UCL, Poisson and Rigid) are compared to the available FE results from Ghoreishi et al. (2007) and analytical results from Argatov (2011).

the ones from the UCL model are practically the same. A very good agreement can be observed throughout the whole response range. The Hertzian contact model in the CCL contact model is obviously able to follow the non linear variation, shown in Fig. 9(d), of the amplitude of the contact band predicted by the refined FE model.

9.3. Example 3

A further 1/6 strand, already studied by Frikha et al. (2013) using a refined FE model (1122 triangular elements over the strand cross section, with significant refinements in the neighborhood of contact points), has been the subject of a parametric analysis to highlight the range of values of the lay angle α_0 in which the hypotheses on the contact model are more important. The strand is characterized by a Poisson coefficient $\nu = 0.30$ and a wire to core diameter ratio $\xi_0 = \frac{d_{w0}}{d_{c0}} = 1$. This rather unrealistic value of ξ_0 will be retained in this work in order to allow for a direct comparison with the results reported by Frikha et al. (2013).

Fig. 10(a) depicts, for the UCL and CCL contact models, the curves of the non-dimensional contact compliance $\bar{C}_{n0}$ as a function of the lay angle α_0. The value of the non-dimensional normal contact compliance ($\bar{C}_{n0}$) is evaluated by considering a nominal value of the wire axial strain equal to $1 \cdot 10^{-3}$. Fig. 10(b)–(d) depict the dimensionless curves giving the direct and cross terms of the strand section stiffness as a function of the lay angle. For direct comparison, the adopted dimensionless forms are the same used by Ghoreishi et al. (2007) and Frikha et al. (2013): $\overline{EA} = \frac{EA}{E\pi R_0^2}$, $\overline{C_T} = \frac{C_T}{E\pi R_0^3}$, $\overline{GJ} = \frac{GJ}{E\pi R_0^4}$.

As it can be appreciated from Fig. 10(a), the UCL model leads to higher values of compliance, with a ratio that changes from a few percent, for lower values of α_0, to about 30% for the rather large maximum value reported in the figure. In spite of this large relative variability, Fig. 10(b)–(d) depict an almost negligible impact in terms of stiffness value of the UCL and CCL models, irrespective of which direct or cross term one looks at. Additionally, both these models give results that are very close to the outcome of the FE model by Frikha et al. (with the CCL being obviously closer since it better reproduces the FE displacement field), while showing a marked difference with respect the results from the other two theoretical models herein considered ("Poisson" and "Rigid").

It can be stressed, as it can also be appreciated from the figures, that there is no large difference in the stiffness predicted by all the models for lay angles up to 10–15°. This is the range in which most strands fall into. For larger values of the lay angle, a refined contact model became essential. These results highlight the range of angles for which including the effect of wire flattening became essential.

9.4. Example 4

As a final example, a different 1/6 strand studied by Ghoreishi et al. (2007) using a FE model is considered. The mesh was more coarse with respect to the one of the FE model in Example 3, since each wire section consisted of 12 finite elements (six 15-node and six 20-node solid elements). Due to this discretization, it is expected that the flattening effects will not be fully captured, differently from the radial contraction induced by Poisson effect.

The same strand has been also studied by Argatov (2011) with an analytical model and by Meng et al. (2016) with a semi-analytical one. A parametric analysis is carried out over the same range of lay angles considered in Example 3. The strand is characterized by a Poisson coefficient $\nu = 0.30$ and a wire to core diameter ratio $\xi_0 = \frac{d_{w0}}{d_{c0}} = 0.947$. To this value of ξ_0 it corresponds through Eq. (8) a maximum value of the lay angle of $\alpha_{0,\max} = 15.4^\circ$ which ensures a radial contact. The results, however, will be plotted in the unrealistic range 0–35° to allow for a direct comparison with the results reported by Argatov (2011).

Fig. 11(a) depicts, for the UCL and CCL contact models, the curves of the non-dimensional contact compliance $\bar{C}_{n0}$ as a function of the lay angle α_0. The value of the non-dimensional normal contact compliance ($\bar{C}_{n0}$) is evaluated by considering a nominal value of the wire axial strain equal to $1 \cdot 10^{-3}$. Fig. 11(b)–(d) depict the curves giving the non-dimensional stiffness terms of the strand section as a function of the lay angle. The same dimensionless forms introduced in Example 3 are used. In Fig. 11(c) two curves (C_{T12} and C_{T21}, where the suffixes give the position in the stiffness matrix of Eq. (12)) are reported for the Argatov (2011) model, since the coupling terms coming from that formulation are not symmetric.

As it can be appreciated, Fig. 11(a) is very similar to Fig. 10(a), and the comments made with reference to such figure apply also here. Also, similar comments as those for Fig. 10(b–d) apply to Fig. 11(b–d) for the impact of the UCL and CCL models on the stiffness terms.

From Fig. 11(b–d), it can also be appreciated how the trend predicted by the proposed analytical model is in good accordance with the one by Argatov (2011). The UCL and CCL models give results that are very close to the outcome of the FE model by Ghoreishi et al. and by Argatov for angles less than 10°. At this value of the lay angle the curve for the UCL and CCL models start to separate from the one accounting only for Poisson effect, highlighting as the flattening effect starts to become comparatively important. In the model by Argatov this happens at larger values of the lay angles (about 20°), see also Argatov's paper. This last aspect justifies the lower value of the stiffness coefficients predicted by the proposed model for large lay angle values.

Since the proposed formulation shares with Argatov (2011) the contact model, the difference in the threshold value of the lay angle which marks the flattening becoming important can be traced to the different kinematic models adopted and in the way the stiffness matrix is computed.

Since, as already highlighted, the FE model is not able to reproduce the effects of flattening, its results lay closer to the curve accounting only for Poisson effect. This curve (labeled as "Poisson" in the figures) is very close to the one reporting the results of the Argatov (2011) model up to a lay angle value of 20–25°, after which also the Argatov model starts experiencing a significant effect due to flattening.

10. Conclusions

The experimental evidence shows that the axial-torsional behavior of a metallic strand is essentially linear under typical service loading. The results and the theoretical developments presented in this work highlight that neglecting the contraction of the external wires helix radius, induced by axial-torsional loads, leads to an overestimate of the elastic stiffness. A better estimate of the stiffness coefficients is possible if the changes in the strand internal geometry are fully accounted for. A possible way to take this aspect into account can be first to state the general problem as a geometrically non linear one, and subsequently linearizing it. However, when this has been done in the literature, a non-symmetric stiffness matrix was obtained, which violates Betti's reciprocal work theorem, at the very base of elastic systems. While this discrepancy has usually little practical consequences for the moderate values of the lay angle typical of most strands, it is nevertheless not satisfying from the theoretical point of view. The source can be typically attributed to an inconsistent linearization of the geometrically non-linear problem.

Focusing on single layer stands with wires in radial contact, a different approach is proposed in this work to account in an energetically consistent way for the contraction of the helix radius of the external wires induced by the loading. The proposed formulation is based on: a) the individual modeling of the wires as linear elastic curved thin rods, b) the modeling of the interaction between the external wires and the core wire as an Hertzian normal contact problem and, c), on a comprehensive internal non-linear kinematic model to relate the generalized strains of the wires to the ones of the strand. This non linear model, which fully accounts for all relevant physical mechanisms leading to a contraction of the helix radius (both the Poisson effect in the wires and the local contact deformations), is subsequently linearized to express the strain energy of the strand in closed form.

Knowledge of the strand strain energy in closed form allowed to obtain, for the first time within this context to the authors' knowledge, a symmetric axial-torsional stiffness matrix. Moreover, the expressions for the terms of the stiffness matrix are remarkably compact and simple, making them an attractive tool for analytical developments and design calculations. Extensive comparisons with experimental, analytical and FE results have shown that the proposed expressions are accurate over a wide range of strand constructions and within a loading range sufficiently extended to cover all practical service conditions.

It is also worth noting that the modularity of the proposed formulation allows to easily change the wire to core contact model leaving all the other aspects the same. This feature, which paves the way to the inclusion of future developments, has been exploited in this work to compare two different approaches to model the normal contact compliance (Uncoupled Contact Layout – UCL, and Coupled Contact Layout – CCL) to a rigid contact model (both with or without the Poisson effect included). The predictions of all these models have been compared to both experimental and FE results.

The results have shown the good performances of the proposed model, that gives a very accurate prediction of the axial stiffness and of the axial-torsional coupling term, being only 3% off the available experimental results. The value of the direct and cross terms of the section stiffness matrix decrease moving from the assumption of a rigid model to one that includes both Poisson and the flattening contraction terms. The assumed contact model has a minor impact on the strand response in the usual range of lay angles (up to 10–15 degrees). This is the range in which most strands fall into. However, for larger values of the lay angle, the contact model is important. These results highlight the range of angles for which including the effect of wire flattening became essential.

Finally, the role of the non-dimensional normal contact compliance has been highlighted, as well as how the contact forces on which it depends can be estimated. Numerical values are provided for the wide range of lay angles 0–35°.

Acknowledgments

This work has been partially supported by MIUR (Italian Ministry of Education, University and Research) under the project "PRIN 2015–2018 Identification and monitoring of complex structural systems".

Appendix A. Assessment of the effect of the wire shear force on the evaluation of the wire-core normal contact force

In this Appendix the effects of including the wire shear forces in the computation of the normal contact force are assessed.

Under the assumptions (1) and (2) in Section 5.1, the vector of external moments per unit of length is null (i.e. $\mathbf{m}(S_0)=\mathbf{0}$), while the vector of external forces per unit of length of the wire centerline can be defined as: $\mathbf{p}(S_0)=\left(-\gamma_0^{-1}p_t,\ -\gamma_0^{-1}p_n,\ 0\right)^T$. Where p_n and p_t are the normal and tangential contact forces per unit of length (see Fig. 3), and γ_0 is the correction coefficient defined in Eq. (22).

Due to the helical symmetry of the axial-torsional problem, the following relations hold true: $\frac{d\mathbf{F}_w(S_0)}{dS_0}=0$ and $\frac{d\mathbf{M}_w(S_0)}{dS_0}=0$. The equilibrium equations of the wire (Eq. (16)), hence, reduce to:

$$\begin{cases} -\kappa_0 F_{w2}-\frac{1}{\gamma_0}p_t=0 \\ \kappa_0 F_{w1}-\tau_0 F_{w3}-\frac{1}{\gamma_0}p_n=0 \\ \tau_0 F_{w2}=0 \\ -\kappa_0 M_{w2}=0 \\ \kappa_0 M_{w1}-\tau_0 M_{w3}-F_{w3}=0 \\ \tau_0 M_{w2}+F_{w2}=0 \end{cases} \tag{A.1}$$

From Eq. (A.1) it comes that: $p_t=0$, $F_{w2}=0$ and $M_{w2}=0$. The only equations which are not identically satisfied in (A.1), hence, are equilibrium to translation in the normal direction (Eq. (A.1)-b) and with respect to rotation about the normal direction (Eq. (A.1)-e), i.e.:

$$\begin{cases} \kappa_0 F_{w1}-\tau_0 F_{w3}-\frac{1}{\gamma_0}p_n=0 \\ \kappa_0 M_{w1}-\tau_0 M_{w3}-F_{w3}=0 \end{cases} \tag{A.2}$$

By solving the (Eq. (A.2)-b) for the shear force F_{w3} and substituting in (A.2-a), the normal contact force p_n can be evaluated as:

$$p_n=\gamma_0\kappa_0 F_{w1}-\gamma_0\tau_0(\kappa_0 M_{w1}-\tau_0 M_{w3}) \tag{A.3}$$

Eq. (A.3) can be compared to the approximate one reported in Section 5.1 (Eq. (23)), here rewritten as $\tilde{p}_n=\gamma_0\kappa_0 F_{w1}$.

Eq. (A.3) coincides with Eq. (23) whenever the torsional and bending moments of the wire are zero. This will happen if, and only if, the torsional (χ_{w1}) and bending (χ_{w3}) curvatures of the wires are also zero, which from Eqs. (40) and (42) requires the torsional curvature of the strand to be $\chi_s=0$. Hence, the exact and approximate equations (Eqs. (A.3) and (23)) coincide in the *fixed-end* case (i.e. a tensile loading case with rotations of both end-sections of the strand restrained, see e.g. Section 9.1).

In the general case of a torsional curvature of the strand $\chi_s\neq 0$, the error on the contact force can be quantified as:

$$\Delta_{pn}=\frac{|p_n-\tilde{p}_n|}{\tilde{p}_n}=\left|\frac{\tau_0 M_{w3}}{F_{w1}}\left(\frac{M_{w1}}{M_{w3}}-\frac{\tau_0}{\kappa_0}\right)\right|\leq\Delta_{pn}^{upp} \tag{A.4}$$

where Δ_{pn}^{upp} will be computed in the following, to avoid cumbersome calculation, under the (easily removable) hypothesis of a wire-core rigid contact model and neglecting the Poisson effect. Under these assumptions, by exploiting the constitutive equations of the wires Eqs. (17)–(20), and the kinematic relations in Eqs. (40), (42) and (53), one can get:

$$\frac{M_{w1}}{M_{w3}}=\frac{\cos(\alpha_0)}{(1+\nu)\sin(\alpha_0)} \tag{A.5}$$

and

$$\frac{M_{w3}}{R_0 F_{w1}}=\frac{\xi_0^2}{4(1+\xi_0)^2}\frac{\sin(\alpha_0)\cos(\alpha_0)R_0\chi_s}{\cos^2(\alpha_0)\varepsilon_s+\sin(\alpha_0)\cos(\alpha_0)R_0\chi_s} \tag{A.6}$$

Furthermore, by exploiting the definitions of geometric normal (κ_0) and torsional (τ_0) curvatures (Eqs. (4) and (5)) the following equation can be obtained:

$$\frac{\tau_0}{\kappa_0}=\frac{\cos(\alpha_0)}{\sin(\alpha_0)} \tag{A.7}$$

Finally, by substituting Eqs. (A.5)–(A.7) into Eq. (A.4), and recalling that (in practice) the axial strain of the strand is a non-negative quantity, i.e.: $\varepsilon_s\geq 0$, we can conclude that the relative error on the normal contact forces in Eq. (A.4) is bounded by the following quantity:

$$\Delta_{pn}^{upp}=\frac{\nu}{1+\nu}\cos^2(\alpha_0)\frac{\xi_0^2}{4(1+\xi_0)^2} \tag{A.8}$$

As an example, by assuming: $\nu=0.3$, $\alpha_0=10^\circ$ and $\xi_0=0.95$, from Eq. (A.8), we get: $\Delta_{pn}^{upp}=1.33\%$.

Appendix B. Evaluation of the mechanical curvatures of the wires

Starting from the torsional rotation of the strand, simply represented through the function $\varphi_s=\varphi_s(x_1)$, the rotations of the wire cross sections can be computed by assuming that they rigidly rotate with the one of the strand, as proposed in Foti and Martinelli (2016):

$$\boldsymbol{\varphi}_w=\boldsymbol{\Lambda}_{0,\mathbf{e}_k}^T\mathbf{i}_1\,\varphi_s \tag{B.1}$$

where: $\boldsymbol{\varphi}_w=(\varphi_1,\varphi_2,\varphi_3)^T$ is a column matrix storing the rotations of the wire cross section with respect to the directions of the Serret–Frenet unit vectors $\{\mathbf{f}_k(S_0)\}$ $(k=1,2,3)$, $\boldsymbol{\Lambda}_{0,\mathbf{e}_k}$ is the rotation matrix in Eq. (3), giving the orientation of the Serret–Frenet unit vectors with respect to the strand attached reference system (SRS), and $\mathbf{i}_1$ is the column matrix: $\mathbf{i}_1=(1,0,0)^T$.

To obtain the wire mechanical curvatures, according to the definition in Eq. (14), it is necessary to derive Eq. (B.1) with respect to the arc-length coordinate S_0. Accounting for the differential relation in Eq. (6), the following expression can be easily obtained from (14):

$$\frac{d\boldsymbol{\varphi}_w}{dS_0}=\cos(\alpha_0)\boldsymbol{\Lambda}_{0,\mathbf{e}_k}^T\mathbf{i}_1\,\chi_s+\frac{d\boldsymbol{\Lambda}_{0,\mathbf{e}_k}^T}{dS_0}\boldsymbol{\Lambda}_{0,\mathbf{e}_k}\boldsymbol{\varphi}_w \tag{B.2}$$

where χ_s is the torsional curvature of the strand, i.e.: $\chi_s=d\varphi_s/dx_1$.

The derivative with respect to S_0 of the rotation matrix $\boldsymbol{\Lambda}_{w0,\mathbf{e}_k}$ gives the variation of the orientation of the Serret–Frenet unit vectors along the helicoidal wire centerline. This variation is controlled by the well-known Serret–Frenet formulae (see e.g. Kreyszig, 1991), which can be expressed as:

$$\frac{d\boldsymbol{\Lambda}_{0,\mathbf{e}_k}}{dS_0}=\boldsymbol{\Lambda}_{0,\mathbf{e}_k}\boldsymbol{\Omega}_0 \tag{B.3}$$

where $\boldsymbol{\Omega}_0$ is the skew symmetric matrix already defined in Eq. (15).

By recalling the properties of skew-symmetric and rotation matrices, and substituting (B.3) in (B.2), the following equation can be obtained:

$$\frac{d\boldsymbol{\varphi}_w}{dS_0}=\cos(\alpha_0)\boldsymbol{\Lambda}_{0,\mathbf{e}_k}^T\mathbf{i}_1\,\chi_s-\boldsymbol{\Omega}_0\boldsymbol{\varphi}_w \tag{B.4}$$

Finally, by substituting (B.4) in (14), the mechanical curvatures of the wire can be expressed as:

$$\boldsymbol{\chi}_w = \cos(\alpha_0)\boldsymbol{\Lambda}^T_{w0,\mathbf{e}_k}\mathbf{i}_1\,\chi_s = \begin{pmatrix} \cos^2(\alpha_0)\chi_s \\ 0 \\ \sin(\alpha_0)\cos(\alpha_0)\chi_s \end{pmatrix} \tag{B.5}$$

Appendix C. Computation of the linearization coefficients

As it has been shown in Section 6, the axial strain of the external wires (ε_w) and the radial contraction parameter (β) are two non-linear functions of the axial strain (ε_s) and torsional curvature (χ_s) of the strand. Linearized expressions for ε_w and β, however, can be obtained through a first-order Taylor's expansion of the functions $\varepsilon_w(\varepsilon_s,\ \chi_s)$ and $\beta(\varepsilon_s,\ \chi_s)$ in the neighborhood of the reference configuration C_0: $\varepsilon_s = 0,\ \chi_s = 0$. These linearized expressions have been introduced in Section 7 as: $\varepsilon_w = A\varepsilon_s + B\chi_s$ (Eq. (56)) and $\beta = 1 + C\varepsilon_s + D\chi_s$ (Eq. (59)). All the steps needed to compute the coefficients A, B, C and D will be presented in the following.

It is first convenient to rewrite the Eq. (55), which implicitly defines the function $\varepsilon_w(\varepsilon_s,\ \chi_s)$, as it follows:

$$\begin{aligned} f(\varepsilon_s,\chi_s,\varepsilon_w) &= \cos^2(\alpha_0)(1+\varepsilon_s)^2 \\ &\quad + \mathcal{B}(\varepsilon_s,\varepsilon_w)^2\sin^2(\alpha_0)\left(1+\frac{R_0\chi_s}{\tan(\alpha_0)}\right)^2 \\ &\quad -(1+\varepsilon_w)^2 = 0 \end{aligned} \tag{C.1}$$

where (see Eqs. (46), (50) and (52)):

$$\begin{aligned} \mathcal{B}(\varepsilon_s,\varepsilon_w) &= \beta_v(\varepsilon_s,\varepsilon_w) + \beta_f(\varepsilon_w) - 1 \\ &= 1 - \frac{\nu}{1+\xi_0}(\varepsilon_s + \xi_0\varepsilon_w) - \frac{2\bar{\delta}_n}{1+\xi_0} \end{aligned} \tag{C.2}$$

It is worth noting that the non-dimensional normal contact approach $\bar{\delta}_n$, which appears in Eq. (C.2), is a non-linear function of the wire axial strain ε_w. This functional dependence can be made explicit, by recalling Eqs. (23), (26) and (30), as: $\bar{\delta}_n = \bar{\delta}_n(\bar{p}_n(p_n(\varepsilon_w)))$.

The partial derivatives of the function $f(\varepsilon_s,\ \chi_s,\ \varepsilon_w)$ can be calculated as:

$$\begin{aligned} \frac{\partial f(\varepsilon_s,\chi_s,\varepsilon_w)}{\partial\varepsilon_s} &= 2\cos^2(\alpha_0)(1+\varepsilon_s) \\ &\quad + 2\mathcal{B}(\varepsilon_s,\varepsilon_w)\sin^2(\alpha_0)\left(1+\frac{R_0\chi_s}{\tan(\alpha_0)}\right)^2\frac{\partial\mathcal{B}(\varepsilon_s,\varepsilon_w)}{\partial\varepsilon_s} \\ \frac{\partial f(\varepsilon_s,\chi_s,\varepsilon_w)}{\partial\chi_s} &= 2\mathcal{B}^2(\varepsilon_s,\varepsilon_w)\sin(\alpha_0)\cos(\alpha_0)R_0\left(1+\frac{R_0\chi_s}{\tan(\alpha_0)}\right) \end{aligned} \tag{C.3}$$

$$\begin{aligned} &\frac{\partial f(\varepsilon_s,\chi_s,\varepsilon_w)}{\partial\varepsilon_w} \\ &= 2\mathcal{B}(\varepsilon_s,\varepsilon_w)\sin^2(\alpha_0)\left(1+\frac{R_0\chi_s}{\tan(\alpha_0)}\right)^2\frac{\partial\mathcal{B}(\varepsilon_s,\varepsilon_w)}{\partial\varepsilon_w} \\ &\quad - 2(1-\varepsilon_w) \end{aligned} \tag{C.4}$$

where:

$$\frac{\partial\mathcal{B}(\varepsilon_s,\varepsilon_w)}{\partial\varepsilon_s} = -\frac{\nu}{1+\xi_0} \tag{C.5}$$

$$\frac{\partial\mathcal{B}(\varepsilon_s,\varepsilon_w)}{\partial\varepsilon_w} = -\frac{\nu\xi_0}{1+\xi_0} - \frac{2}{(1+\xi_0)}\frac{\partial\bar{\delta}_n}{\partial\varepsilon_w} \tag{C.6}$$

The derivative $\frac{\partial\bar{\delta}_n}{\partial\varepsilon_w}$ can be easily evaluated through the chain rule: $\frac{\partial\bar{\delta}_n}{\partial\varepsilon_w} = \frac{\partial\bar{\delta}_n}{\partial\bar{p}_n}\frac{\partial\bar{p}_n}{\partial p_n}\frac{\partial p_n}{\partial\varepsilon_w}$. Hence, by exploiting the Eqs. (23), (26), (36), and recalling the definitions of γ_0 (Eq. (22)) and κ_0 (Eq. (4)), the Eq. (C.6) can also be rewritten as:

$$\frac{\partial\mathcal{B}(\varepsilon_s,\varepsilon_w)}{\partial\varepsilon_w} = -\frac{\nu\xi_0}{1+\xi_0} - \frac{2\left(1-\nu^2\right)\xi_0^2\sin^2(\alpha_0)\bar{C}_n(\bar{p}_n(\varepsilon_w))}{(1+\xi_0)\left(1+\xi_0\left(1-\sin^2(\alpha_0)\right)\right)} \tag{C.7}$$

Starting from Eqs. (C.1)–(C.5) and (C.7), it can be easily verified that the function $f(\varepsilon_s,\ \chi_s,\ \varepsilon_w)$ is continuous with continuous derivatives in $\varepsilon_s,\ \chi_s,\ \varepsilon_w$. Hence, by application of the Dini's theorem on implicit functions (see e.g. Dontchev and Rockafellar, 2014) the partial derivatives of the function $\varepsilon_w(\varepsilon_s,\ \chi_s)$, which is implicitly defined by Eq. (C.1), can be evaluated as:

$$\frac{\partial\varepsilon_w(\varepsilon_s,\ \chi_s)}{\partial\varepsilon_s} = -\frac{\frac{\partial f(\varepsilon_s,\chi_s,\varepsilon_w(\varepsilon_s,\chi_s))}{\partial\varepsilon_s}}{\frac{\partial f(\varepsilon_s,\chi_s,\varepsilon_w(\varepsilon_s,\chi_s))}{\partial\varepsilon_w}} \tag{C.8}$$

and:

$$\frac{\partial\varepsilon_w(\varepsilon_s,\ \chi_s)}{\partial\chi_s} = -\frac{\frac{\partial f(\varepsilon_s,\chi_s,\varepsilon_w(\varepsilon_s,\chi_s))}{\partial\chi_s}}{\frac{\partial f(\varepsilon_s,\chi_s,\varepsilon_w(\varepsilon_s,\chi_s))}{\partial\varepsilon_w}} \tag{C.9}$$

The two equations above are well defined in the reference configuration C_0 ($\varepsilon_s = 0,\ \chi_s = 0$), since $\left.\frac{\partial f(\varepsilon_s,\chi_s,\varepsilon_w(\varepsilon_s,\chi_s))}{\partial\varepsilon_w}\right|_{C_0} \neq 0$. Evaluation of the Eqs. (C.8) and (C.9) in the reference configuration C_0, then, allows to easily calculate the linearization coefficients A and B as:

$$\begin{aligned} A &= \left.\frac{\partial\varepsilon_w(\varepsilon_s,\ \chi_s)}{\partial\varepsilon_s}\right|_{C_0} = -\frac{\left.\frac{\partial f(\varepsilon_s,\chi_s,\varepsilon_w(\varepsilon_s,\chi_s))}{\partial\varepsilon_s}\right|_{C_0}}{\left.\frac{\partial f(\varepsilon_s,\chi_s,\varepsilon_w(\varepsilon_s,\chi_s))}{\partial\varepsilon_w}\right|_{C_0}} \\ &= \frac{\cos^2(\alpha_0) - \frac{\nu\sin^2(\alpha_0)}{1+\xi_0}}{1 + \frac{\nu\xi_0\sin^2(\alpha_0)}{1+\xi_0} + \frac{2\left(1-\nu^2\right)\xi_0^2\bar{C}_{n0}\sin^4(\alpha_0)}{(1+\xi_0)\left(1+\xi_0\left(1-\sin^2(\alpha_0)\right)\right)}} \end{aligned} \tag{C.10}$$

$$\begin{aligned} B &= \left.\frac{\partial\varepsilon_w(\varepsilon_s,\ \chi_s)}{\partial\chi_s}\right|_{C_0} = -\frac{\left.\frac{\partial f(\varepsilon_s,\chi_s,\varepsilon_w(\varepsilon_s,\chi_s))}{\partial\chi_s}\right|_{C_0}}{\left.\frac{\partial f(\varepsilon_s,\chi_s,\varepsilon_w(\varepsilon_s,\chi_s))}{\partial\varepsilon_w}\right|_{C_0}} \\ &= \frac{\sin(\alpha_0)\cos(\alpha_0)R_0}{1 + \frac{\nu\xi_0\sin^2(\alpha_0)}{1+\xi_0} + \frac{2\left(1-\nu^2\right)\xi_0^2\bar{C}_{n0}\sin^4(\alpha_0)}{(1+\xi_0)\left(1+\xi_0\left(1-\sin^2(\alpha_0)\right)\right)}} \end{aligned} \tag{C.11}$$

where $\bar{C}_{n0}$ denotes the value of the non-dimensional wire-to-core normal contact compliance in the reference configuration C_0 (see also Section 5.3).

Once the coefficients A and B are known, the linearization coefficients C and D can be simply evaluated through derivation of Eq. (C.2). By recalling Eq. (54), a straightforward application of the chain rule leads to the following results:

$$\begin{aligned} C &= \left.\frac{\partial\beta(\varepsilon_s,\ \chi_s)}{\partial\varepsilon_s}\right|_{C_0} = \left.\frac{\partial\mathcal{B}(\varepsilon_s,\varepsilon_w)}{\partial\varepsilon_s}\right|_{C_0} + A\left.\frac{\partial\mathcal{B}(\varepsilon_s,\varepsilon_w)}{\partial\varepsilon_w}\right|_{C_0} \\ &= -\frac{\nu}{1+\xi_0} - \frac{2\left(1-\nu^2\right)\xi_0^2\sin^2(\alpha_0)\bar{C}_{n0}}{(1+\xi_0)\left(1+\xi_0\left(1-\sin^2(\alpha_0)\right)\right)}A \end{aligned} \tag{C.12}$$

$$\begin{aligned} D &= \left.\frac{\partial\beta(\varepsilon_s,\ \chi_s)}{\partial\chi_s}\right|_{C_0} = B\left.\frac{\partial\mathcal{B}(\varepsilon_s,\varepsilon_w)}{\partial\varepsilon_w}\right|_{C_0} \\ &= -\frac{2\left(1-\nu^2\right)\xi_0^2\sin^2(\alpha_0)\bar{C}_{n0}}{(1+\xi_0)\left(1+\xi_0\left(1-\sin^2(\alpha_0)\right)\right)}B \end{aligned} \tag{C.13}$$

References

Argatov, I., 2001. Solution of the plane hertz problem. J. Appl. Mech. Tech. Phys. 42, 1064–1072.

Argatov, I., 2011. Response of a wire rope strand to axial and torsional loads: asymptotic modeling of the effect of interwire contact deformations. Int. J. Solids Struct. 48, 1413–1423.

Blouin, F., Cardou, A., 1989. A study of helically reinforced cylinders under symmetric loads and application to strand mathematical modeling. Int. J. Solids Struct. 25, 189–200.

Cappa, P., 1988. An experimental study of wire strains in an undamaged and damaged steel strand subjected to tensile load. Exp. Mech. 28, 346–349.

Cardou, A., Jolicoeur, C., 1997. Mechanical models of helical strands. Appl. Mech. Rev. (ASME) 50, 1–14.

Chen, Y., Meng, F., Gong, X., 2017. Full contact analysis of wire rope strand subjected to varying loads based on semi-analytical method. Int. J. Solids Struct. 117, 51–66.

Costello, G.A., 1990. Theory of Wire Ropes. Springer-Verlag, New York, USA.

Dontchev, A.L., Rockafellar, R.T., 2014. Implicit Functions and Solution Mappings. Springer-Verlag, New York, USA.

Elata, D., Eshkenazy, R., Weiss, M.P., 2004. The mechanical behavior of a wire rope with an independent wire rope core. Int. J. Solids Struct. 41, 1157–1172.

Feyrer, K., 2007. Wire Ropes: Tension, Endurance, Reliability. Springer-Verlag, Berlin, Germany.

Foti, F., de Luca di, R.A., 2016. Analytical and finite element modeling of the elastic–plastic behavior of metallic strands under axial-torsional loads. Int. J. Mech. Sci. 115–116, 202–214.

Foti, F., de Luca di, R.A., Martinelli, L., 2017. modeling the axial-torsional response of metallic strands accounting for the deformability of the internal contact surfaces. In: AIMETA 2017 – Proceedings of the 23rd Conference of the Italian Association of Theoretical and Applied Mechanics, Vol. 3, pp. 323–330.

Foti, F., Martinelli, L., 2016. Mechanical modeling of metallic strands subjected to tension, torsion and biaxial bending. Int. J. Solids Struct. 91, 1–17.

Frigerio, M., Buehlmann, P.B., Buchheim, J., Holdsworth, S.R., Dinser, S., Franck, C.M., Papailiou, K., Mazza, E., 2016. Analysis of the tensile response of a stranded conductor using a 3d finite element model. Int. J. Mech. Sci. 106, 176–183.

Frikha, A., Cartraud, P., Treyssède, F., 2013. Mechanical modeling of helical structures accounting for translational invariance. Part 1: Static behavior. Int. J. Solids Struct. 50, 1373–1382.

Ghoreishi, S.R., Messager, T., Cartraud, P., Davies, P., 2007. Validity and limitations of linear analytical models for steel wire strands under axial loading, using a 3d FE model. Int. J. Mech. Sci. 49, 1251–1261.

Goudreau, S., Charette, F., Hardy, C., Cloutier, L., 1998. Bending energy dissipation of simplified single-layer stranded cable. J. Eng. Mech. (ASCE) 124, 811–817.

Huang, N.C., 1973. Theories of elastic slender curved rods. J. Appl. Math. Phys. (ZAMP) 24, 1–19.

Huang, N.C., 1978. Finite extension of an elastic strand with a central core. J. Appl. Mech. (ASME) 45, 852–859.

Jiang, W.G., Yao, M.S., Walton, J.M., 1999. A concise finite element for simple straight wire rope strand. Int. J. Mech. Sci. 41, 143–161.

Johnson, K., 1985. Contact Mechanics. Cambridge University Press, Cambridge, UK.

Judge, R., Yang, Z., Jones, S.W., Beattie, G., 2012. Full 3d finite element modeling of spiral strand cables. Constr. Build. Mater. 35, 452–459.

Karathanasopoulos, N., Angelikopoulos, P., 2016. Optimal structural arrangements of multilayer helical assemblies. Int. J. Solids Struct. 78, 1–8.

Karathanasopoulos, N., Ganghoffer, J.F., Papailiou, K.O., 2016. Analytical closed-form expressions for the structural response of helical constructions to thermal loads. Int. J. Mech. Sci. 117, 258–264.

Karathanasopoulos, N., Kress, G., 2015. Mechanical response of a helical body to axial, torsional and radial strain. Int. J. Mech. Sci. 94–95, 260–265.

Karathanasopoulos, N., Reda, H., Ganghoffer, J.F., 2017. Finite element modeling of the elastoplastic axial-torsional response of helical constructions to traction loads. Int. J. Mech. Sci. 133, 368–375.

Knapp, R.H., 1979. Derivation of a new stiffness matrix for helically armoured cables considering tension and torsion. Int. J. Numer. Methods Eng. 14, 515–529.

Kreyszig, E., 1991. Differential Geometry. Dover Publications, New York, USA.

Kumar, K., Botsis, J., 2001. Contact stresses in multilayered strands under tension and torsion. J. Appl. Mech. (ASME) 68, 432–440.

Kumar, K., Cochran, J.E., 1987. Closed-form analysis for elastic deformations of multilayered strands. Trans. ASME 54, 898–903.

Lanteigne, J., 1985. Theoretical estimation of the response of helically armored cables to tension, torsion and bending. J. Appl. Mech. (ASME) 52, 423–432.

Lee, W.K., 1991. An insight into wire rope geometry. Int. J. Solids Struct. 28, 471–490.

Leech, C.M., 2002. The modeling of friction in polymer fibre ropes. Int. J. Mech. Sci. 44, 621–643.

Leissa, A.W., 1959. Contact stresses in wire ropes. Wire Wire Prod. 34 (307–314), 372–373.

Love, A.E.H., 1944. A Treatise on the Mathematical Theory of Elasticity, Fourth ed. Dover Publications, New York, USA.

Machida, S., Durelli, A.J., 1972. Response of a strand to axial and torsional displacements. The Institute of Ocean Science and Engineering, The Catholic University of America, Report 72-1, Washington D.C., USA

Meng, F., Chen, Y., Du, M., Gong, X., 2016. Study on effect of inter-wire contact on mechanical performance of wire rope strand based on semi-analytical method. Int. J. Mech. Sci. 115–116, 416–427.

Onur, Y.A., 2016. Experimental and theoretical investigation of prestressing steel strand subjected to tensile load. Int. J. Mech. Sci. 118, 91–100.

Raoof, M., 1983. Interwire Contact Forces and the Static Hysteretic and Fatigue Properties of Multi-Layer Structural Strands. Imperial College of Science and Technology, London, UK Doctoral Dissertation.

Raoof, M., Hobbs, R.E., 1988. Analysis of multilayered structural strands. J. Eng. Mech. (ASCE) 114, 1166–1182.

Raoof, M., Kraincanic, I., 1994. Critical examination of various approaches used for analysing helical cables. J. Strain Anal. Eng. Des. 29, 43–55.

Rawlins, C.B., 2005. Analytical Elements of Overhead Conductor Fabrication. Fultus Books, Palo Alto CA USA.

Roark, R.J., 1965. Formulas for Stress and Strain, Fourth ed. McGraw-Hill.

Sathikh, S., Moorthy, M.B.K., Krishnan, M., 1996. A symmetric linear elastic model for helical wire strands under axisymmetric loads. J. Strain Anal. 31, 389–399.

Spak, K., Agnes, G., Inman, D., 2013. Cable modeling and internal damping developments. Appl. Mech. Rev. (ASME) 65 (010801), 1–18.

Starkey, W.L., Cress, H.A., 1959. An analysis of critical stresses and mode of failure of a wire rope. J. Eng. Ind. (ASME) 81, 307–316.

Treyssède, F., 2016. Dispersion curve veering of longitudinal guided waves propagating inside prestressed seven-wire strands. J. Sound Vib. 367, 56–68.

Urchegui, M.A., Tato, W., Gómez, X., 2008. Wear evolution in a stranded rope subjected to cyclic bending. J. Mater. Eng. Perform. 17, 550–560.

Utting, W.S., 1984. Experimental and Theoretical Studies of Stresses and Deformation of Wire Ropes Under Axial Tensile Loads. University of Liverpool, UK Doctoral Dissertation.

Utting, W.S., Jones, N., 1985. Tensile testing of a wire rope strand. J. Strain Anal. Eng. Des. 20, 151–164.

Utting, W.S., Jones, N., 1987. The response of wire rope strands to axial tensile loads – part i. Experimental results and theoretical predictions. Int. J. Mech. Sci. 29, 605–619.

Utting, W.S., Jones, N., 1987. The response of wire rope strands to axial tensile loads – part II. Comparison of experimental results and theoretical predictions. Int. J. Mech. Sci. 29, 621–636.

Velinsky, A., Anderson, G.L., Costello, G.A., 1984. Wire rope with complex cross sections. J. Eng. Mech. (ASCE) 110, 380–391.

Xiang, L., Wang, H.Y., Chen, Y., Guan, Y.J., Dai, L.H., 2017. Elastic-plastic modeling of metallic strands and wire ropes under axial tension and torsion loads. Int. J. Solids Struct. 129, 103–118.

Yu, Y., Chen, Z., Liu, H., Wang, X., 2014. Finite element study of behavior and interface force conditions of seven-wire strand under axial and lateral loading. Constr. Build. Mater. 66, 10–18.